

## Integration of Noise and Coda Correlation Data into Kinematic and Waveform Inversions

Project Officer: William Vandermeer

Total Project Funding: \$1,406,745

April 24, 2013

Daniel R.H. O'Connell, PhD

Fugro Consultants

Modeling

## Project Objectives

- Obtain high-accuracy (10 m or less) absolute geothermal field earthquake locations and complete moment tensors that identify fault/shear-planes, and also map fractures estimate fully-coupled poro-elastic stresses to improve EGS performance, accurately position wells, reduce costs, and minimize seismic risks.
- Develop and validate strategies for passive data acquisition and processing that minimize costs while maximizing resolution of geothermal reservoir fractures and stresses in 4D.
- Provide these capabilities as readily available transformational technologies from multiple commercial sources to support geothermal exploration and production.
- Provide fully-coupled 3D waveform inversion and poro-elastic modeling capabilities that run overnight to support near-real-time analyses during EGS stimulations to allow adjustments that minimize seismic risks while improving EGS stimulation performance.

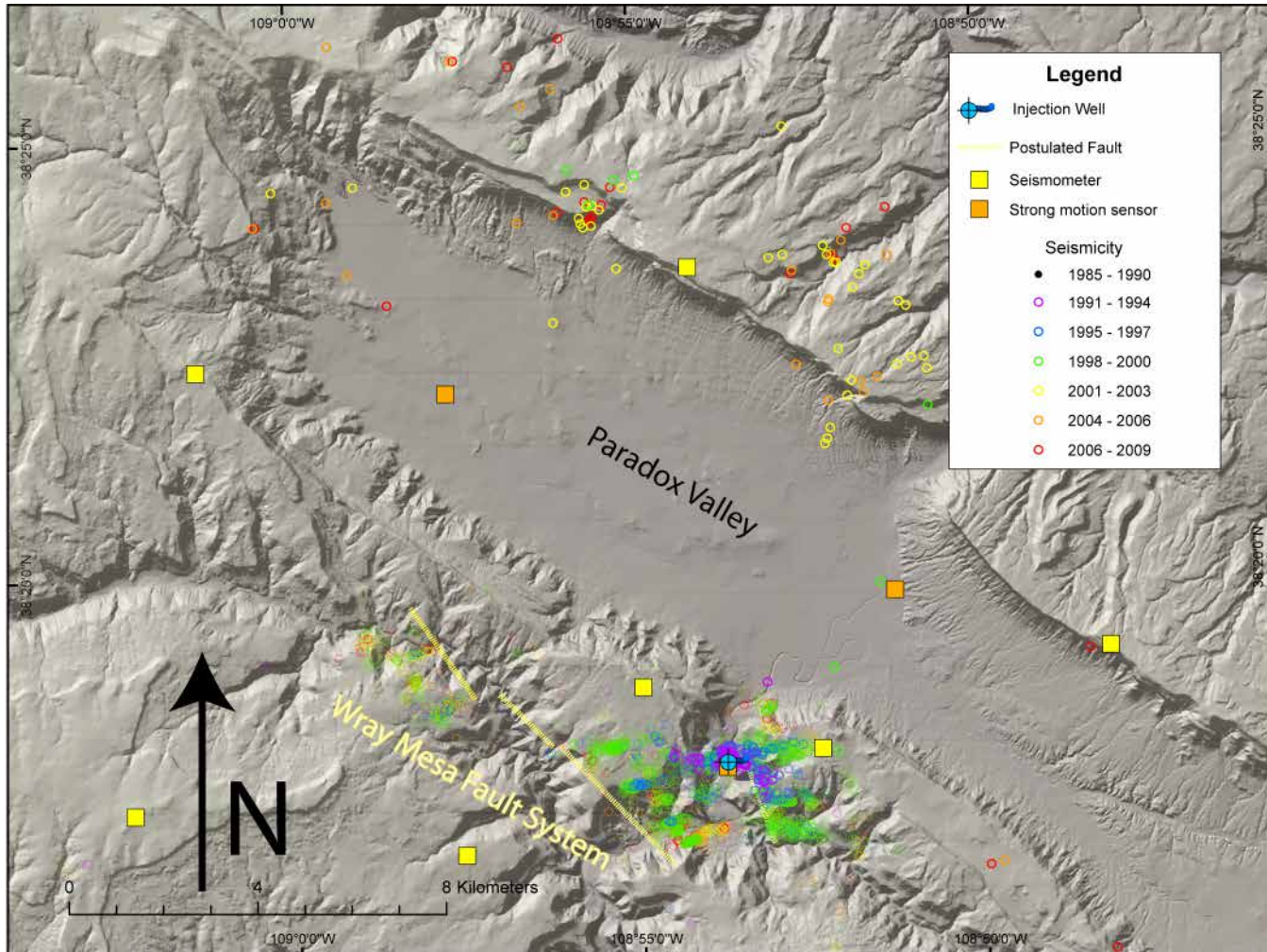
- Develop reciprocity-based MPI/GPU-optimized adjoint approach for 3D Frechet waveform inversion kernels with 3D viscoelastic variable and discontinuous finite-difference mesh to reduce memory requirements by 87% over uniform meshes and accounts for topography for direct body-wave modeling using data functionals (Gee and Jordan, 1992).
- Extend coda-wave theory to quantify velocity-resolution performance as a function of source separation, focal mechanism variability, and frequency to establish and validate the foundation for tomographic inversion for 4D velocity changes on the order of 0.1% or more.

- Bayesian S-wave arrival-time picking using eigenvector decomposition and a robust characteristic impulsive arrival identifier (Lomax et al., 2012) to obtain realistic S-wave picks and most crucially, realistic picking uncertainties to use in residual weighted (L1) inversions.
- Use station-by-station generalized inversion of absolute and relative times to improve accuracy of absolute arrival times by an order of magnitude to obtain higher resolution 3D velocity structure and absolute hypocenter locations using standard L1 weighted 3D velocity-hypocenter inversion with station terms to solve for station time shift uncertainties in a unified inversion.

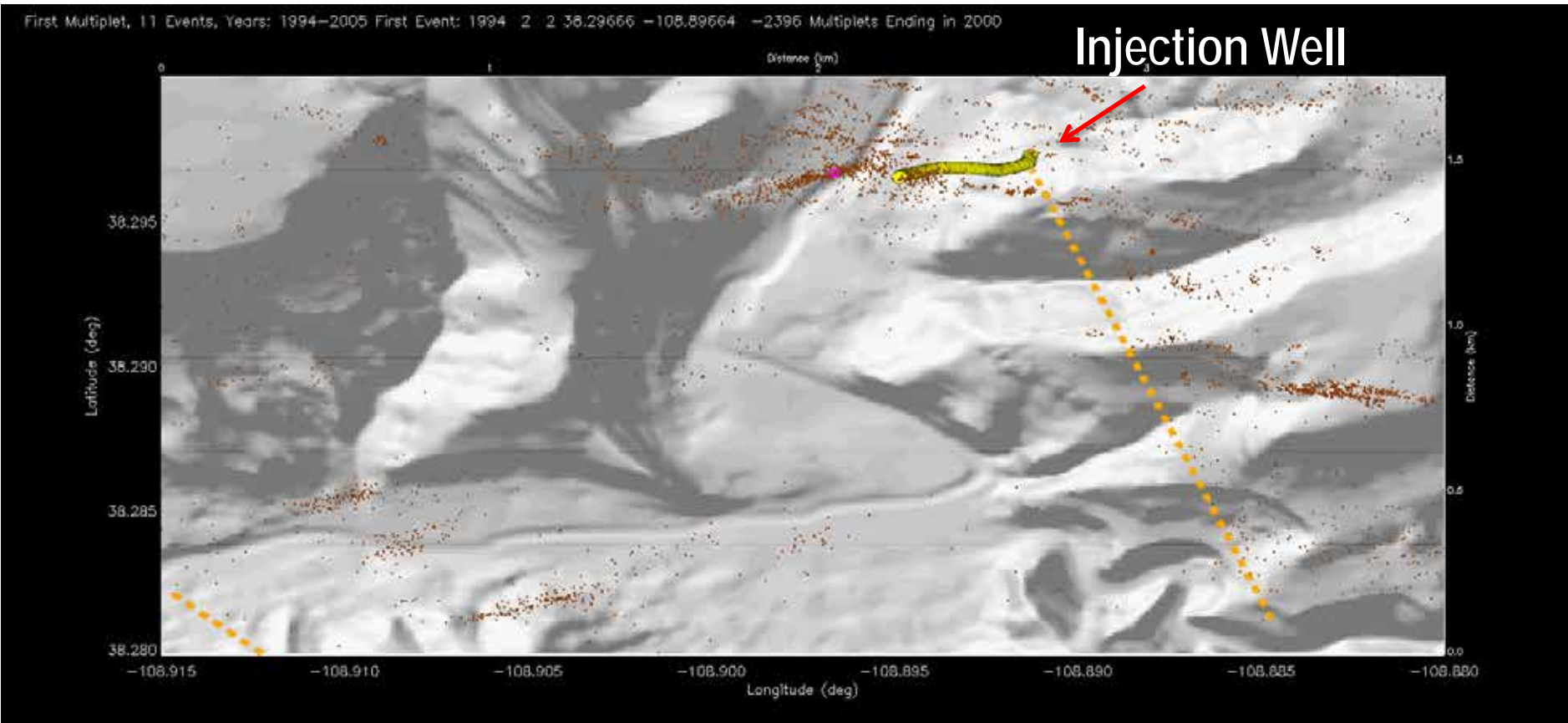
- Use Tikhonov regularization (Petrov, 2002) deconvolution with ambient noise and stationary phase coda wave estimation of surface-wave dispersion from 0.5 to 5 Hz at network stations. We developed IMASW (O'Connell and Turner, 2011) to obtain 200 m depth resolution of shear-wave velocities at seismic stations in about an hour per station using non-intrusive sources and ambient noise.
- Integrate surface wave dispersion constraints into 3D travel-time inversion 3D velocity-interface depth inversion (Rawlinson and Urvoy, 2006) to accurately represent shallow velocity structure and station site responses for waveform inversion.

- Exploit oil/gas investment in commercialized joint 3D travel-time-gravity tomography that accounts for topography to incorporate earthquake data (including solving for earthquake locations).
- Exploit oil/gas investment in commercialized acoustic active-source waveform inversion technology that accounts for topography to incorporate earthquake data (including solving for earthquake locations and moment tensors).

Validation of Coda Wave Interferometry: Detection of Velocity Changes near Injection Wells.  
Paradox Valley, Colorado, Injection Well and Induced Seismicity As Function of Time

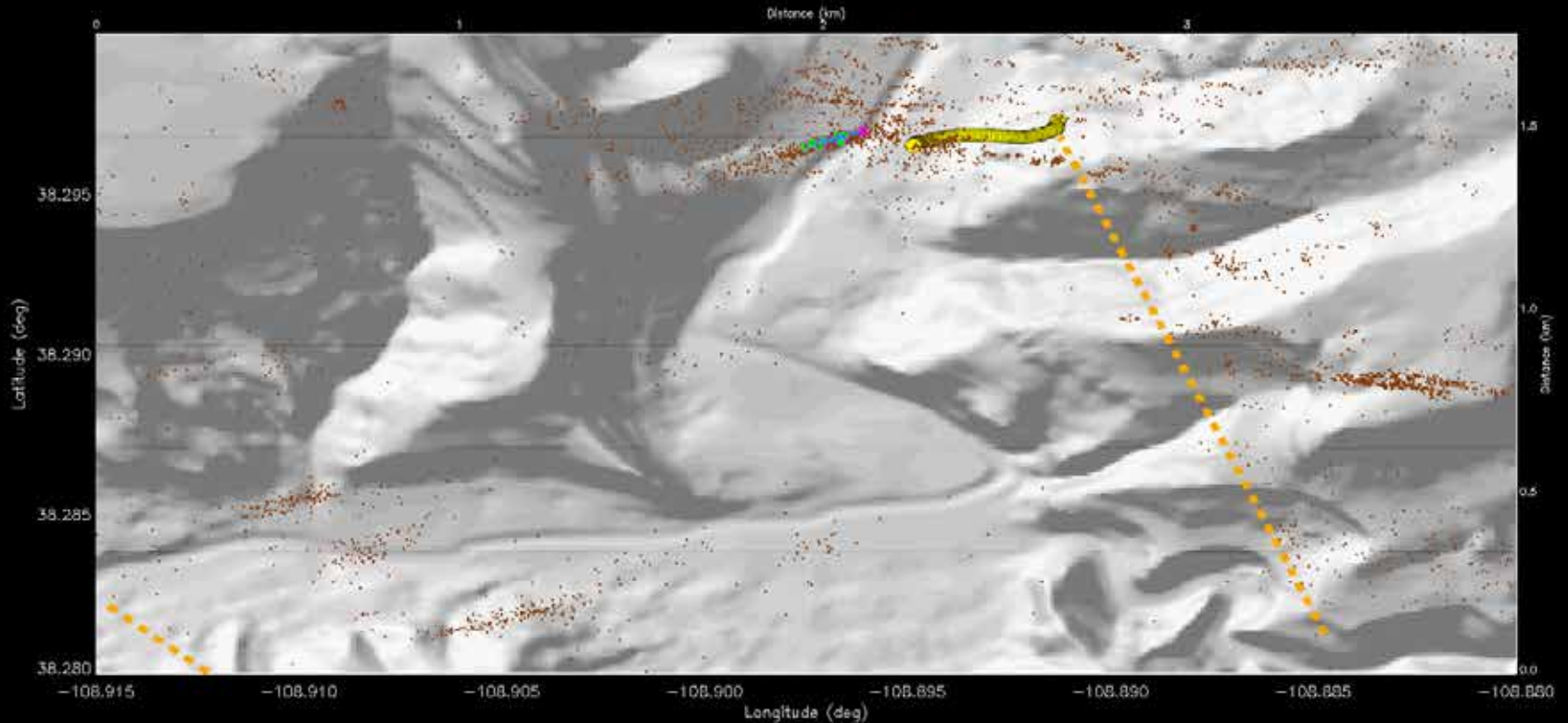


Validation of Coda Wave Interferometry: Detection of Velocity Changes near Injection Wells: Paradox Case  
Click through the next 8 slides to set the evolution of Paradox multiplets over time-space. Magenta circle is current multiplet set and blue lines link successive multiplets in time. (Multiplets = 5 events within 25 m)



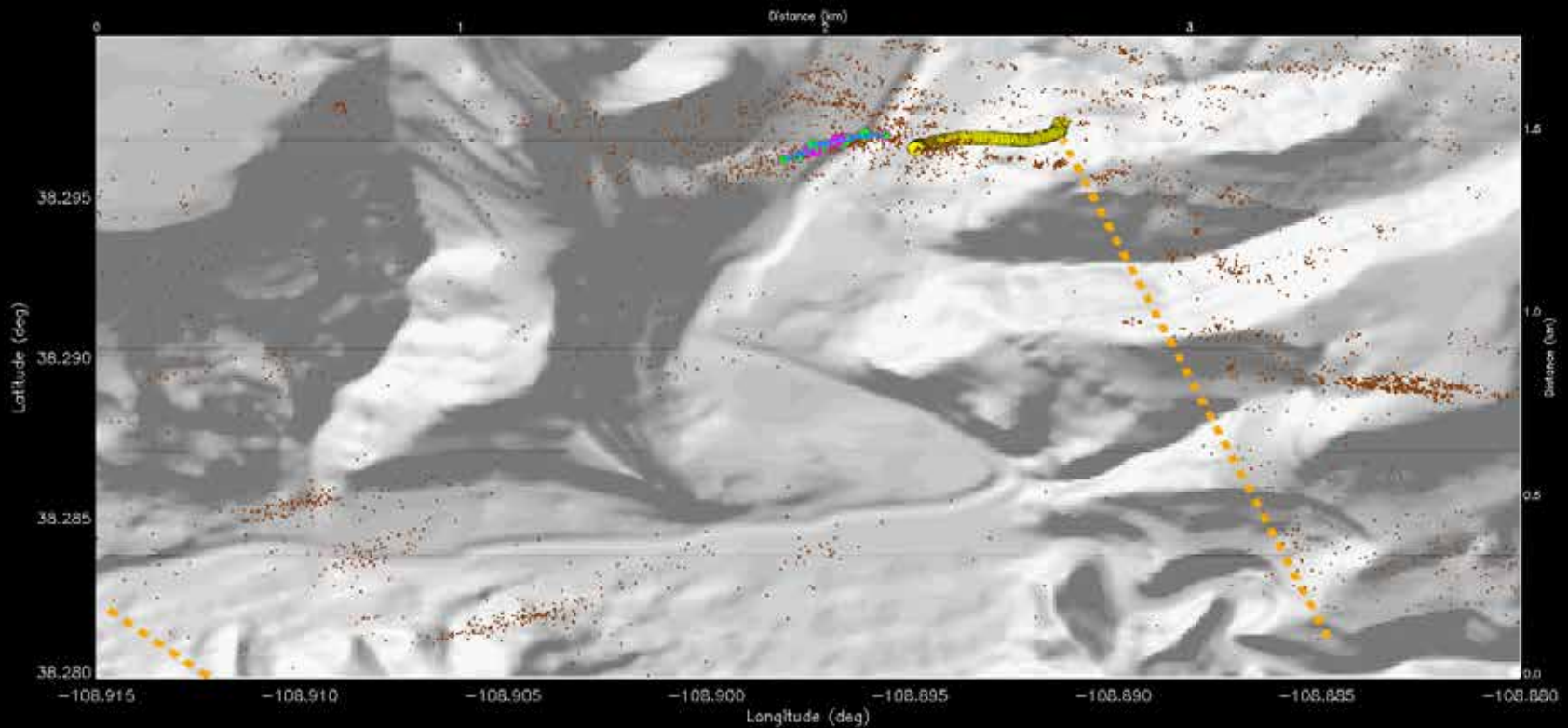
## Validation of Coda Wave Interferometry: Detection of Velocity Changes near Injection Wells. Multiplet set 9 (frame 2 of 8)

Set 9: Delay = 0.23 days, 7 Events, Years: 1994–2008 First Event: 1994 9 23 38.28694 -108.89611 -2413 Multiplets Ending in 2000



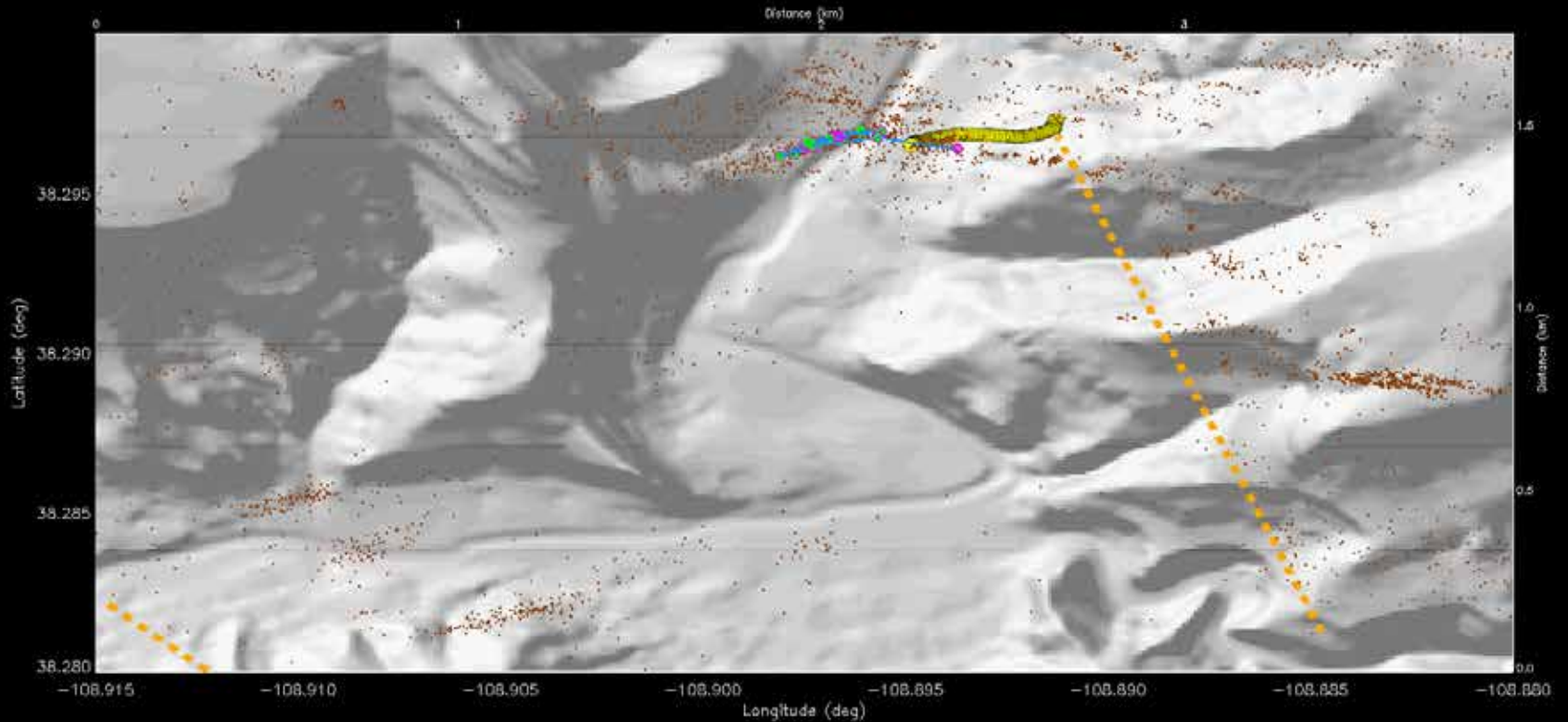
## Validation of Coda Wave Interferometry: Detection of Velocity Changes near Injection Wells. Multiplet set 25 (frame 3 of 8)

Set 25: Delay = 0.00 days, 8 Events, Years: 1997–2006 First Event: 1997 2 28 38.29670 -108.89688 -2354 Multiplets Ending in 2000



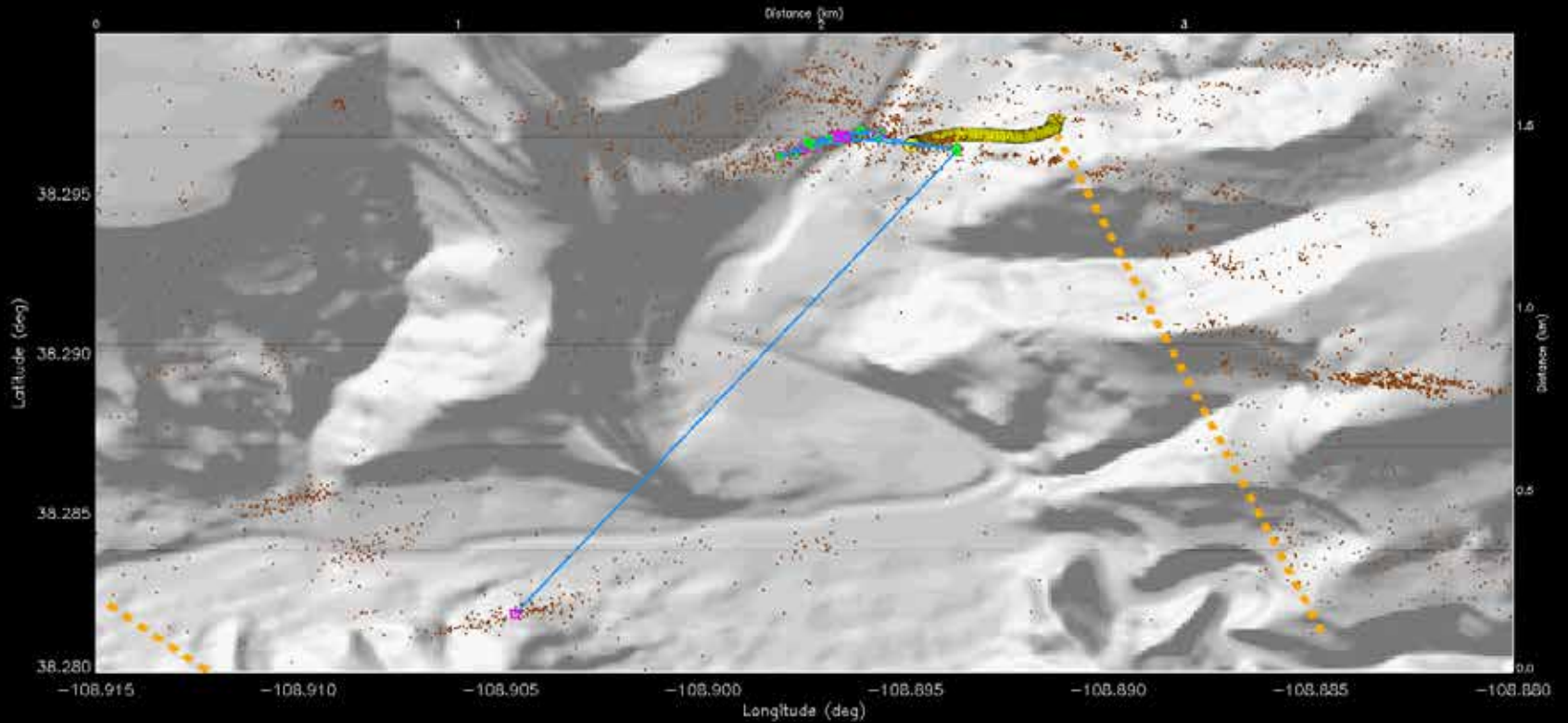
## Validation of Coda Wave Interferometry: Detection of Velocity Changes near Injection Wells. Multiplet set 30 (frame 4 of 8)

Set 30: Delay = 172.58 days, 5 Events, Years: 1998–2005 First Event: 1998 10 17 38.29638 -108.89372 -2595 Multiplets Ending in 2000



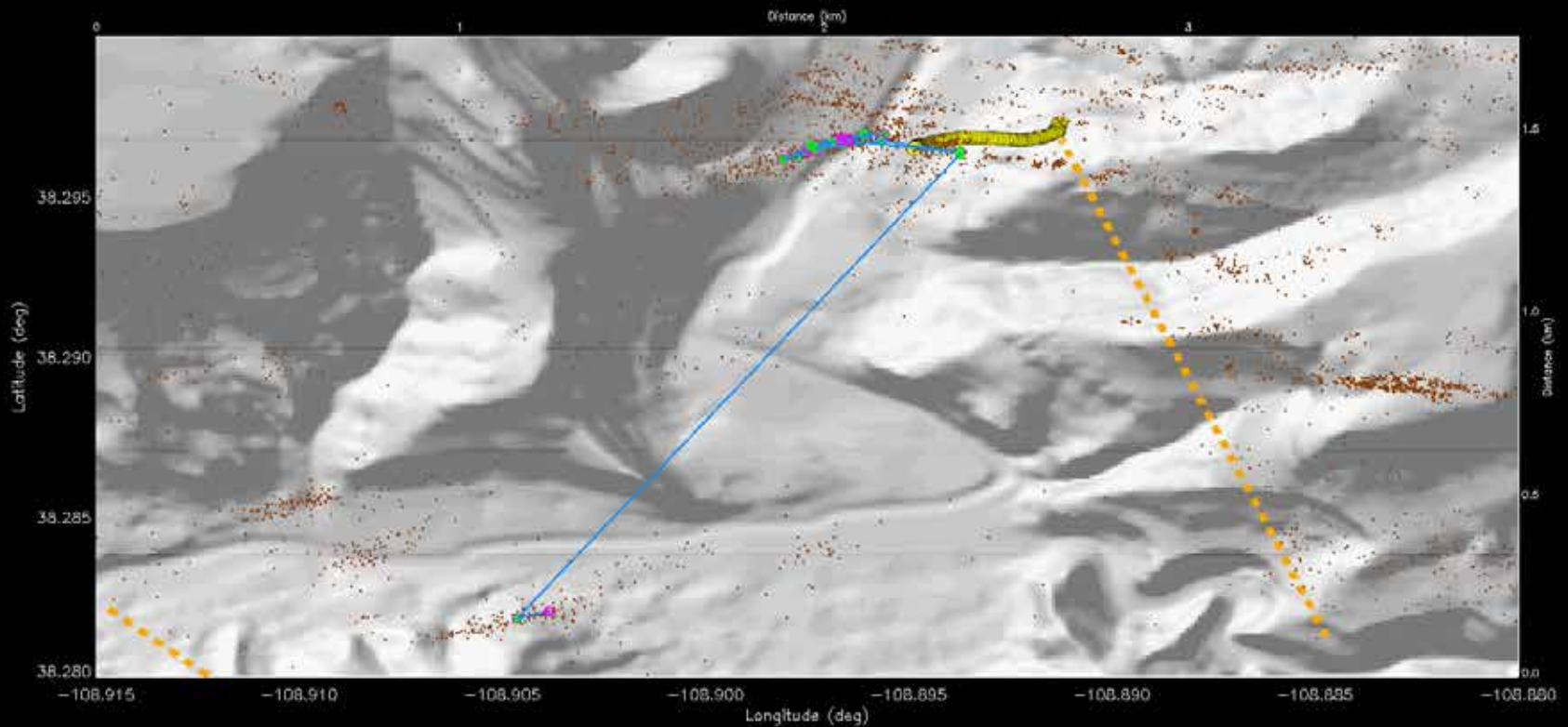
## Validation of Coda Wave Interferometry: Detection of Velocity Changes near Injection Wells. Multiplet set 32 (frame 5 of 8)

Set 32: Delay = 30.05 days, 4 Events, Years: 1999–2005 First Event: 1999 3 25 38.28182 -108.90465 -1527 Multiplets Ending in 2000



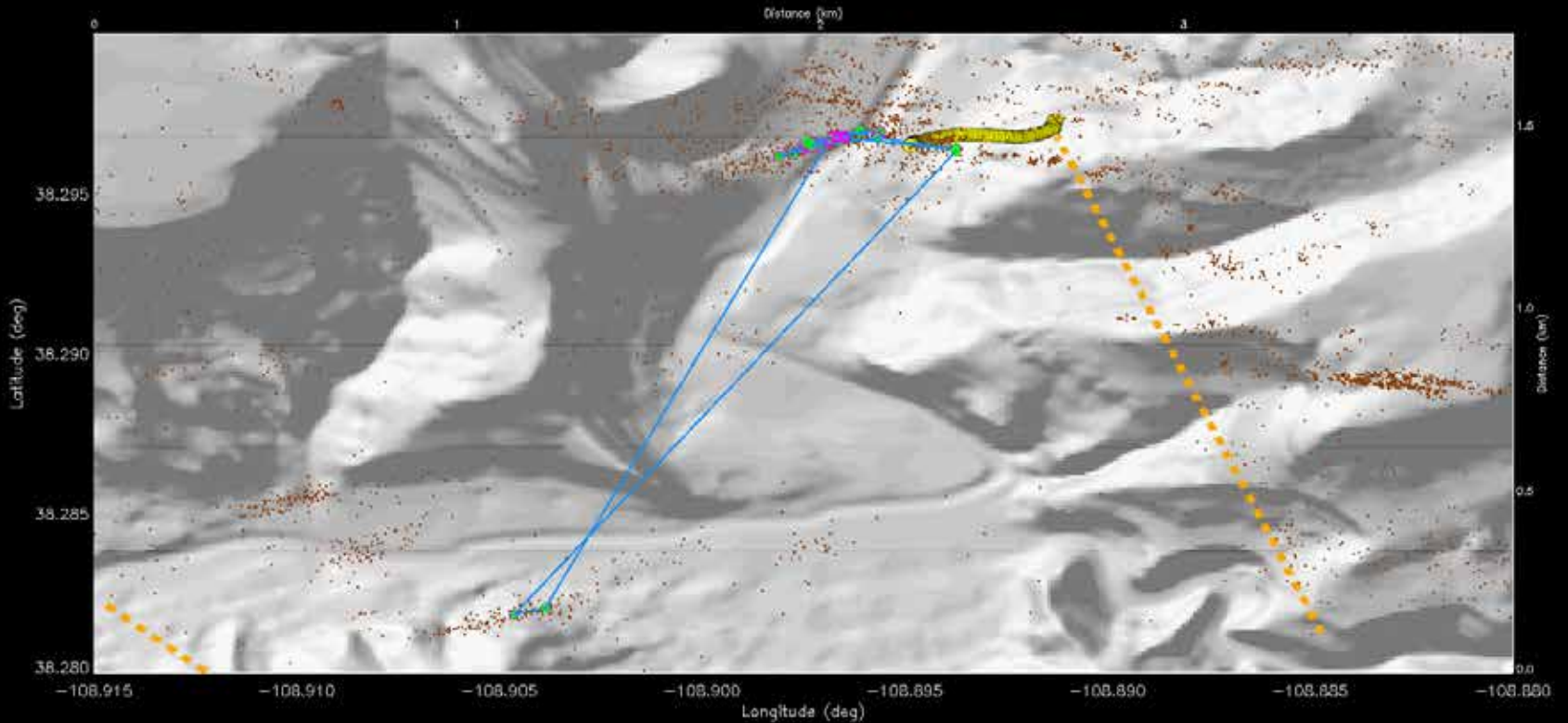
## Validation of Coda Wave Interferometry: Detection of Velocity Changes near Injection Wells. Multiplet set 33 (frame 6 of 8)

Set 33: Delay = 58.62 days, 5 Events, Years: 1999–2004 First Event: 1999 5 22 38.28205 -108.90387 -1534 Multiplets Ending in 2000



## Validation of Coda Wave Interferometry: Detection of Velocity Changes near Injection Wells. Multiplet set 34 (frame 7 of 8)

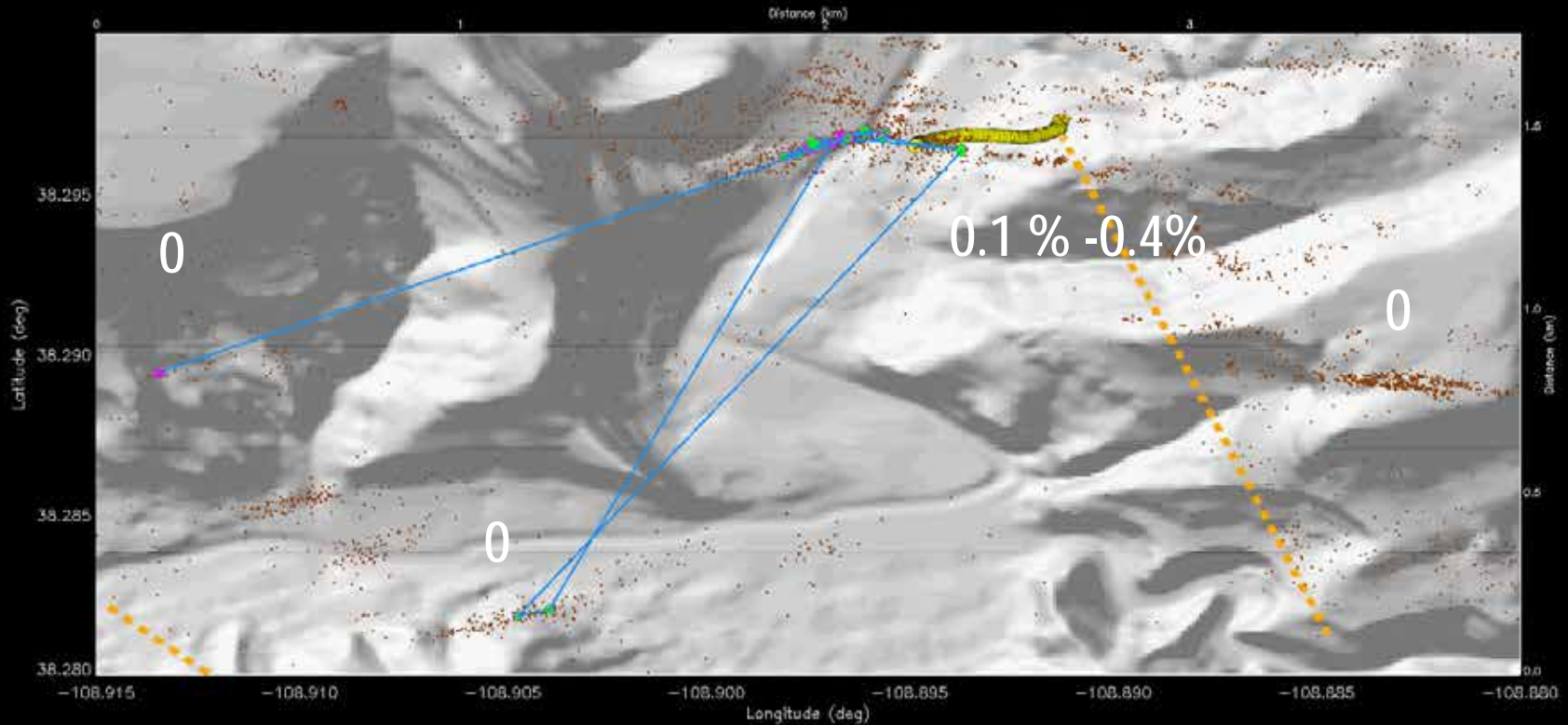
Set 34: Delay = 142.30 days, 6 Events, Years: 1999–2006 First Event: 1999 10 12 38.29662 -108.89689 -2356 Multiplets Ending in 2000



Validation of Coda Wave Interferometry: Detection of 0.1%-0.4% Velocity Changes with 200 m of the Paradox Valley Injection Well. No velocity changes results for multiplets located > 1 km from the well.

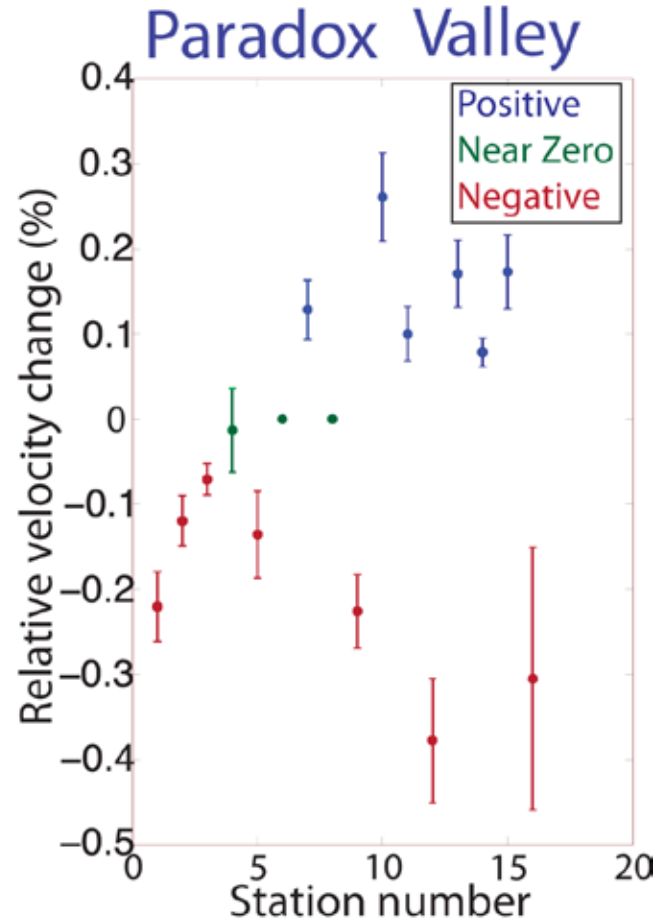
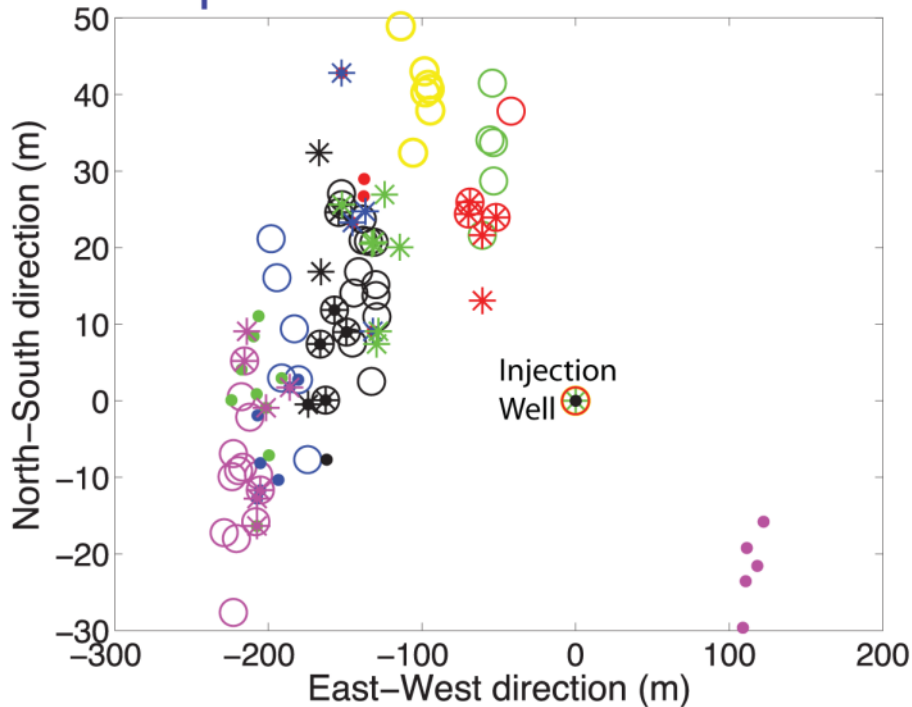
Multiplet set 34 (last frame 8 of 8)

Set 35: Delay = 321.45 days, 4 Events, Years: 2002-2004 First Event: 2002 10 7 38.28941 -108.91346 -2280 Multiplets Ending in 2000



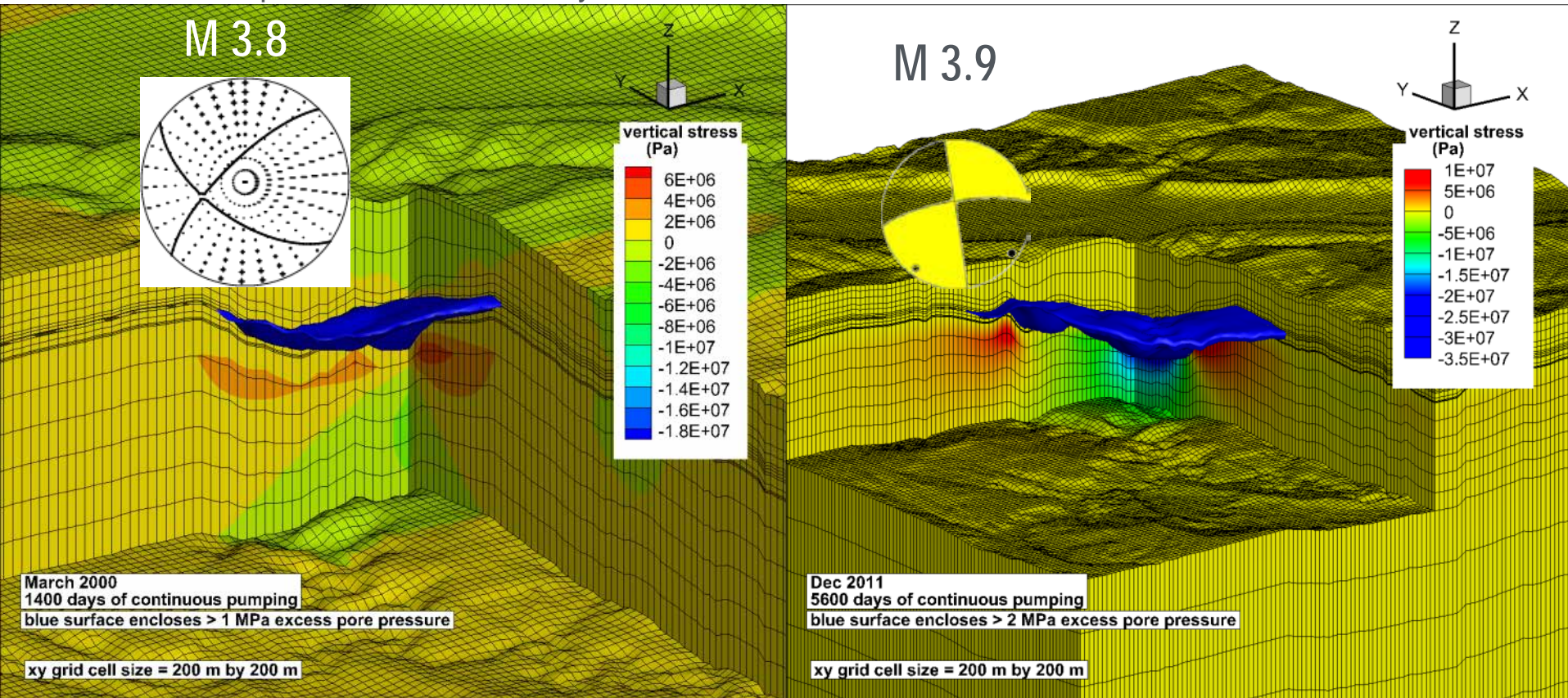
Validation of Coda Wave Interferometry: Detection of 0.1%-0.4% velocity changes within 200 m of the Paradox Valley Injection Well. Testing also confirmed null results for multiplets located > 1 km from the well.

## Multiplet locations for Paradox



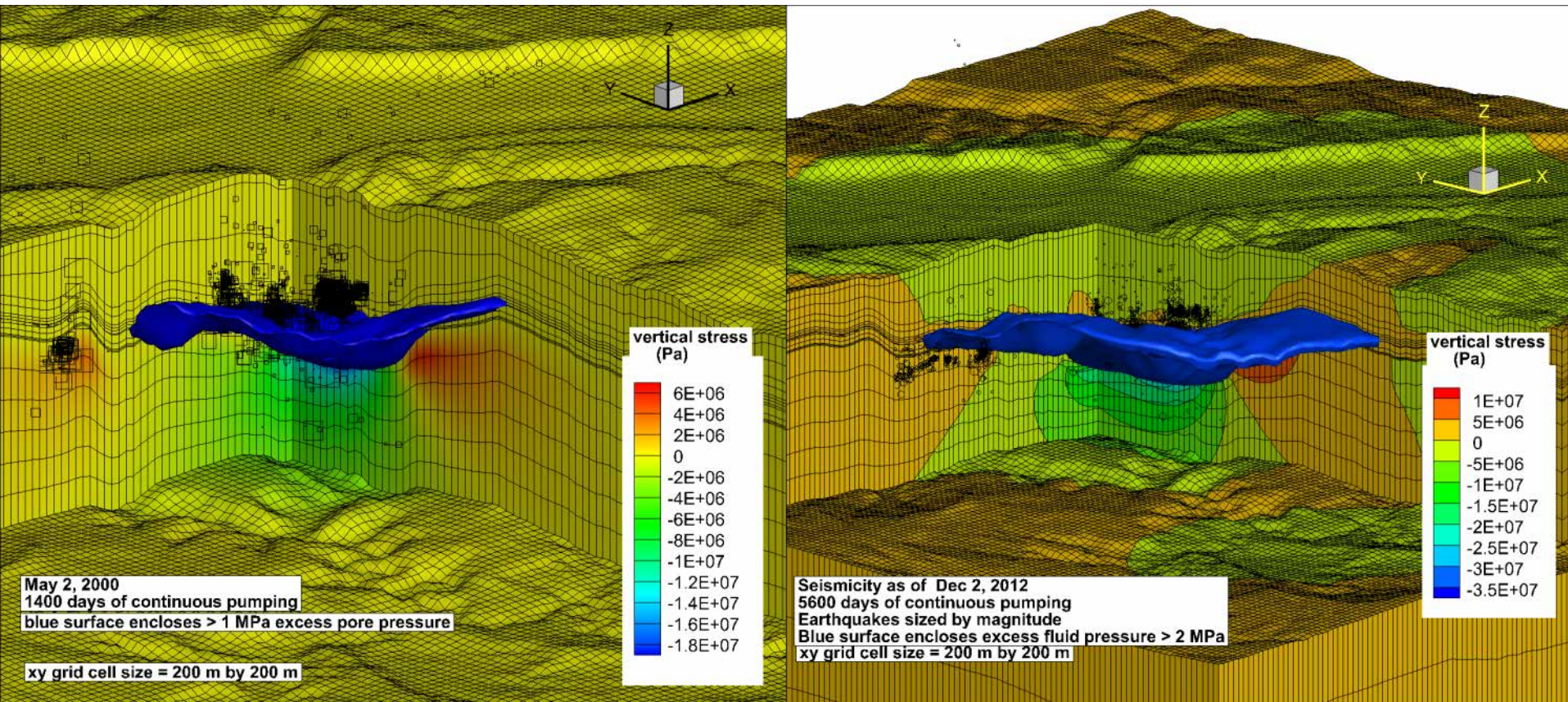
# Accomplishments, Results and Progress

Validation of fully-coupled finite-element solution to Biot's equations consisting of a stress equilibrium equation with a volumetric component composed of pore pressure gradients, and a continuity equation for the pore fluid which contains a volumetric strain component produced by solid displacements. The two equations are coupled through the volumetric strain in the solid. Consistent with locations of largest induced earthquakes at Paradox Valley

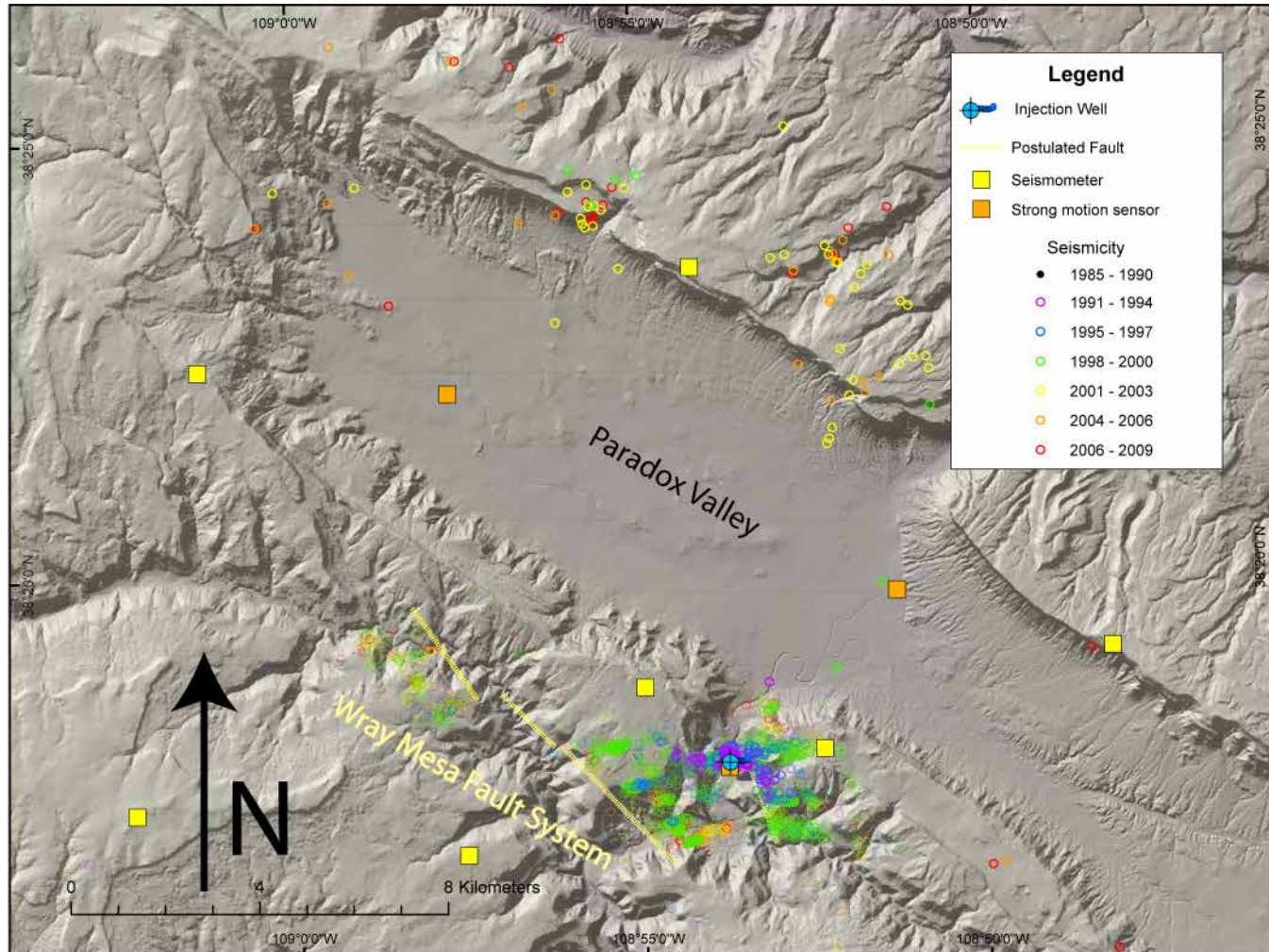


# Accomplishments, Results and Progress

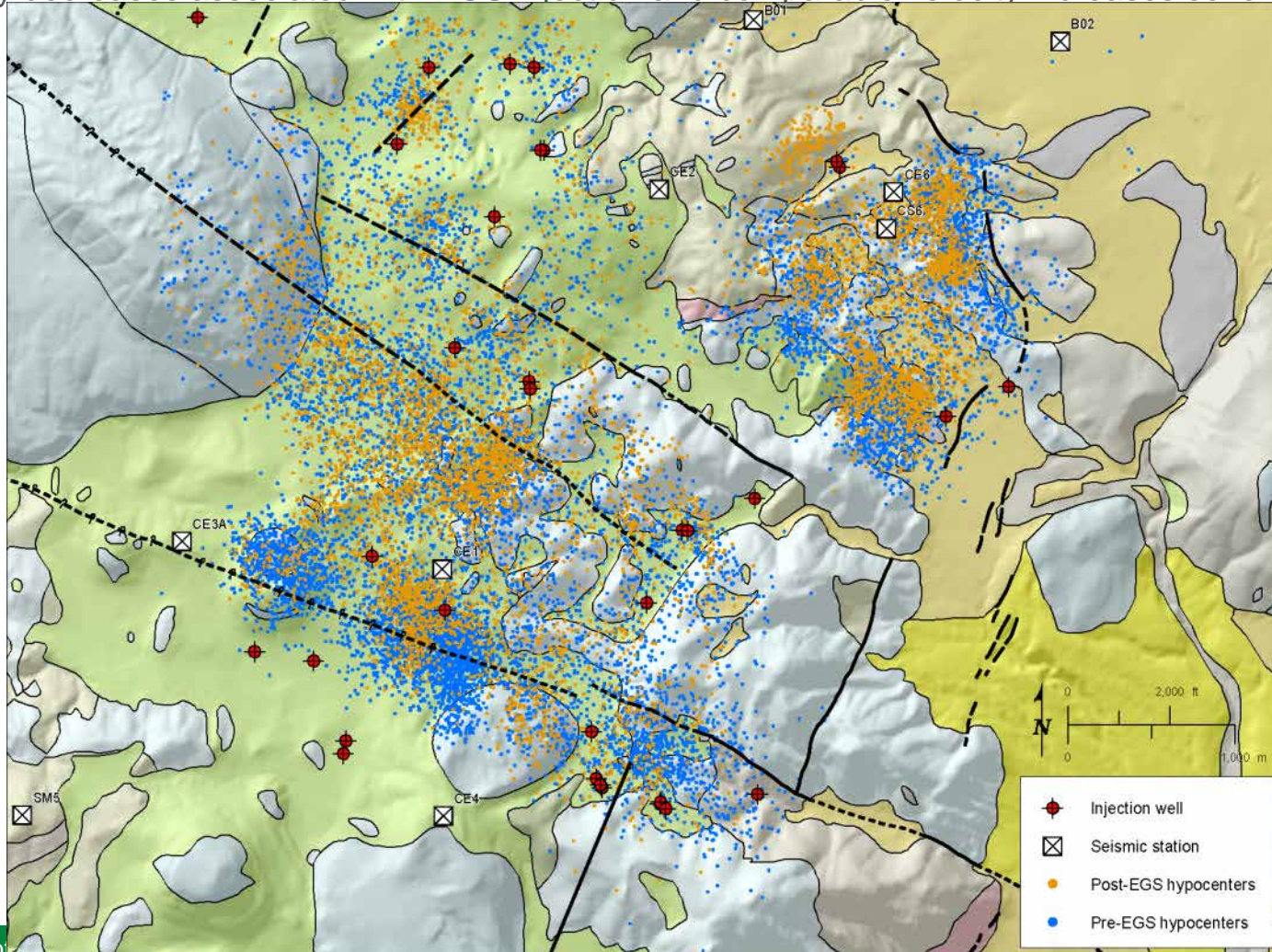
Validation of fully-coupled finite-element solution to Biot's equations consisting of a stress equilibrium equation with a volumetric component composed of pore pressure gradients, and a continuity equation for the pore fluid which contains a volumetric strain component produced by solid displacements. The two equations are coupled through the volumetric strain in the solid. Consistent with Paradox 4D seismicity.



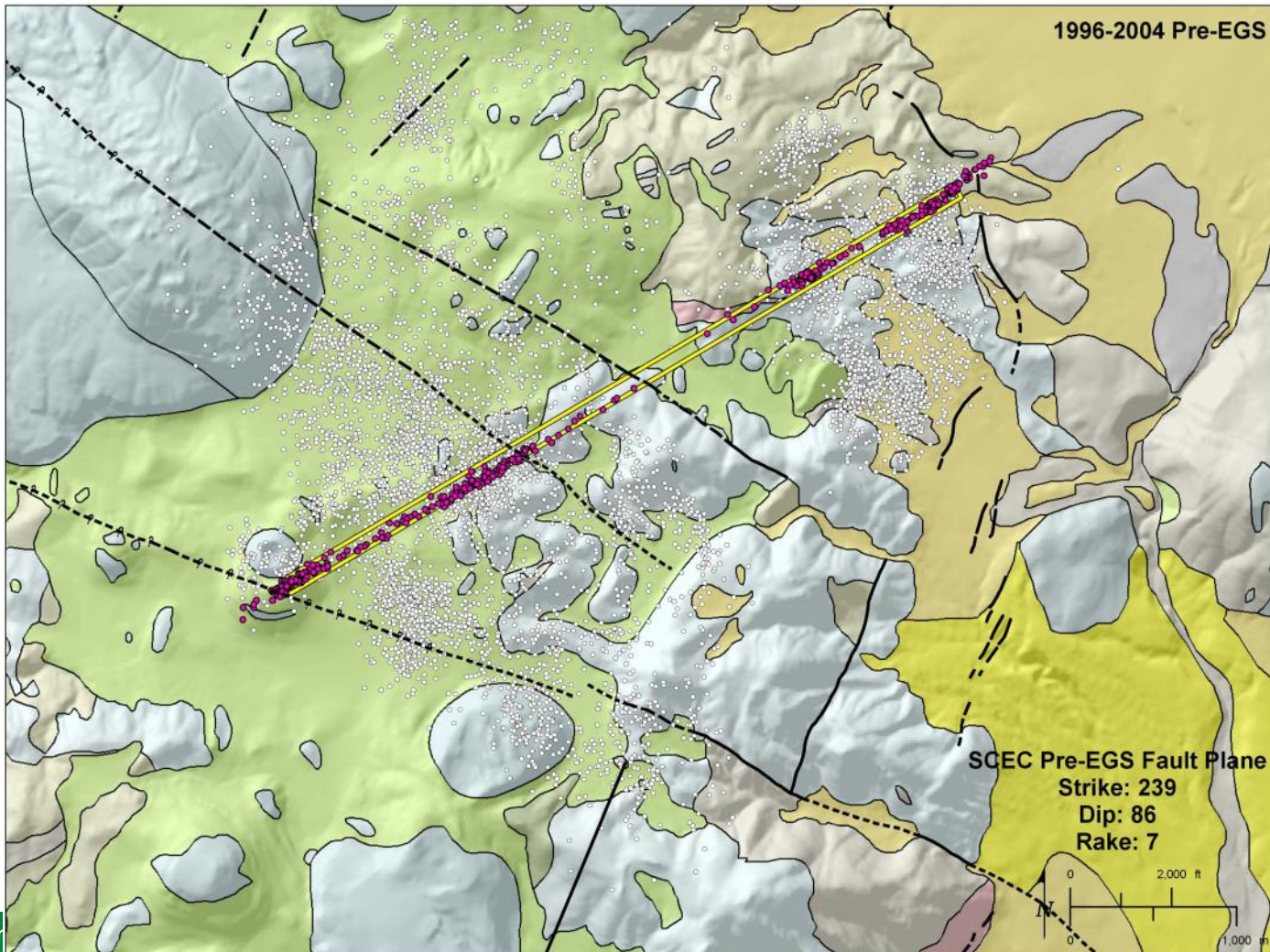
Validation of Coda Wave Interferometry: Detection of Velocity Changes near Injection Wells.  
Paradox Valley, Colorado, Injection Well and Induced Seismicity As Function of Time



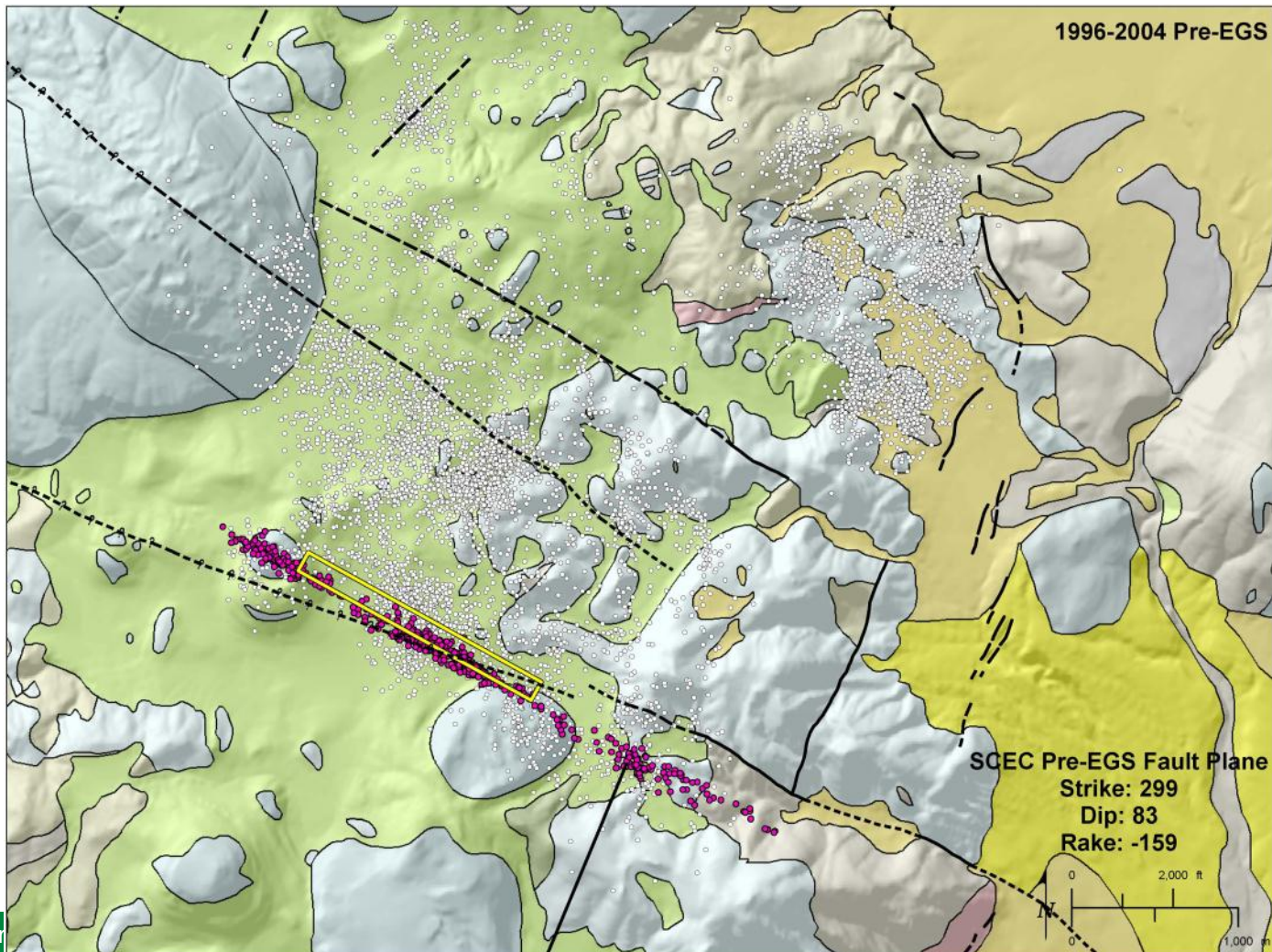
Geothermal application of coda-wave interferometry, Bayesian S-wave picking, and focal mechanisms analyses to the Coso Geothermal field. 87% of all relocated hypocenters are located with 25 m of fault planes delineated by SCEC focal mechanisms of larger earthquakes from 1982-2000. Coda-waves detected 0.1%-0.2% velocity decreases associated with EGS injection and comparable velocity increases several years later.



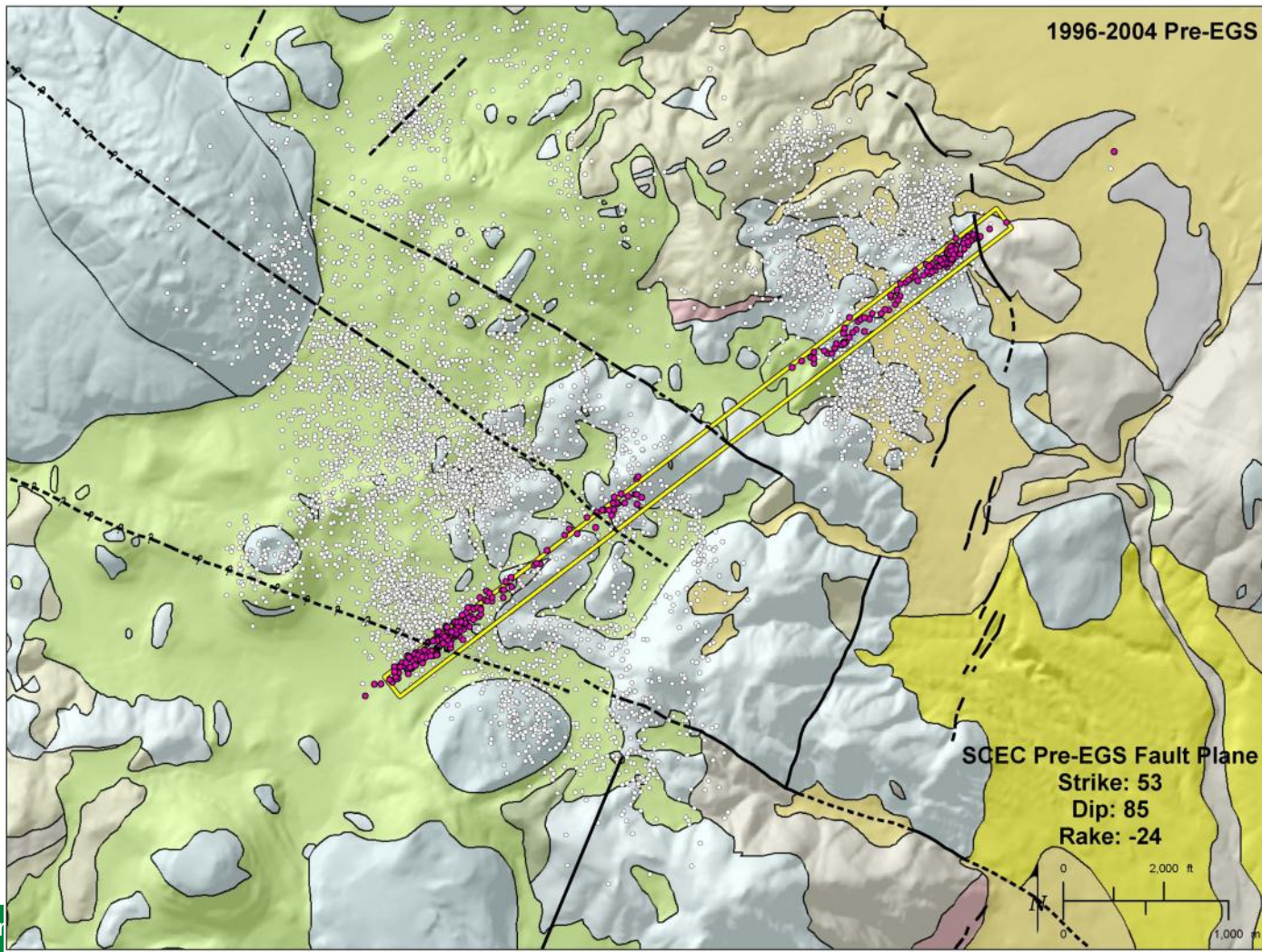
Coso geothermal seismicity is NOT diffuse. 87% occurs within 25 m of planes consistent with tectonic processes along the eastern California shear zone with 83% on vertical and dipping conjugate strike slip planes, 12% normal on planes with dips of 35-70 degrees, and 5% reverse-oblique on steeply-dipping planes. Click on this and next 17 images to animate the different fault planes. (1 of 18) PRE-EGS



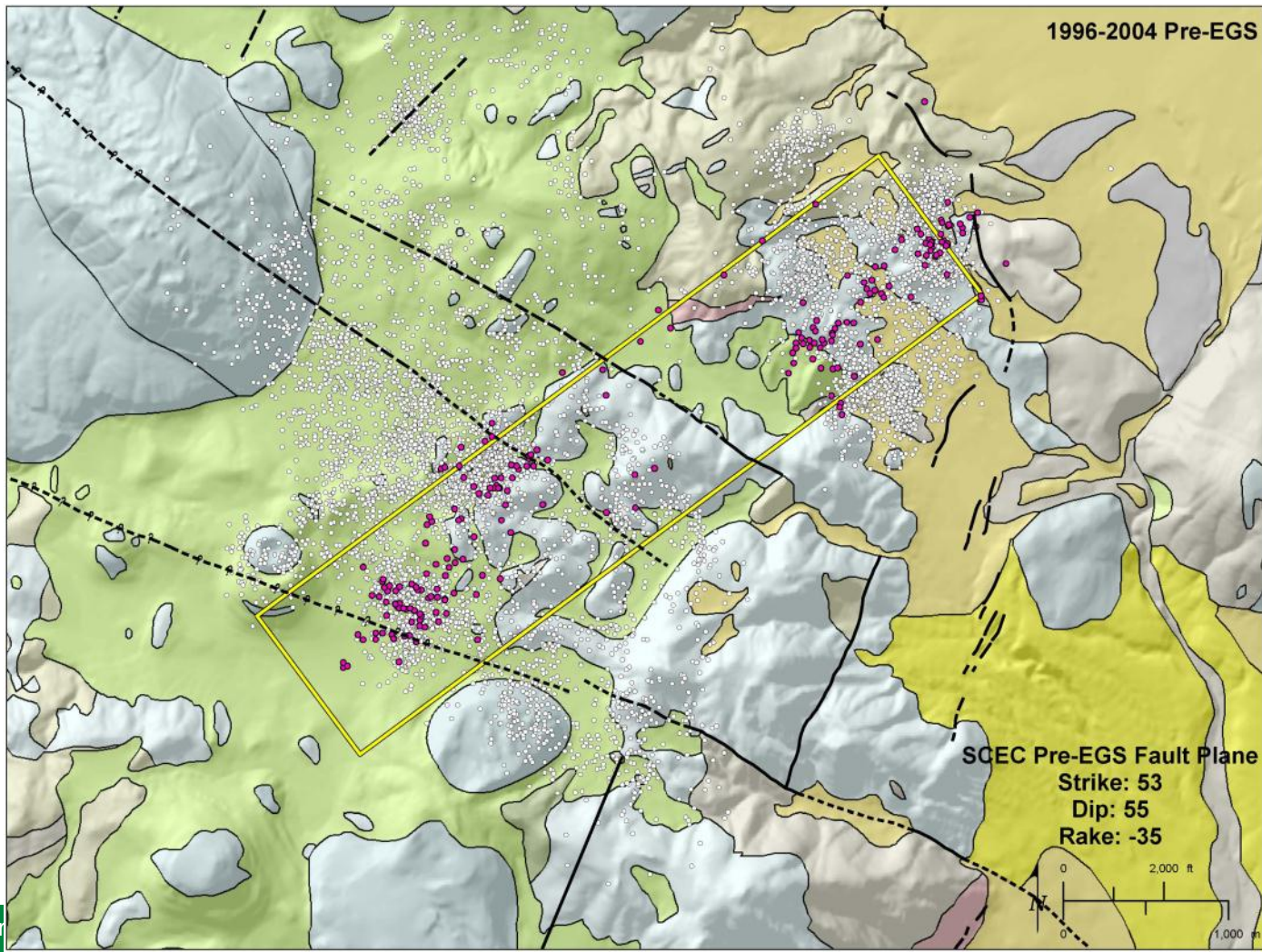
Coso geothermal seismicity is NOT diffuse. 87% occurs within 25 m of planes consistent with tectonic processes along the eastern California shear zone with 83% on vertical and dipping conjugate strike slip planes, 12% normal on planes with dips of 35-70 degrees, and 5% reverse-oblique on steeply-dipping planes. Click on this and next 16 images to animate the different fault planes. (2 of 18) PRE-EGS



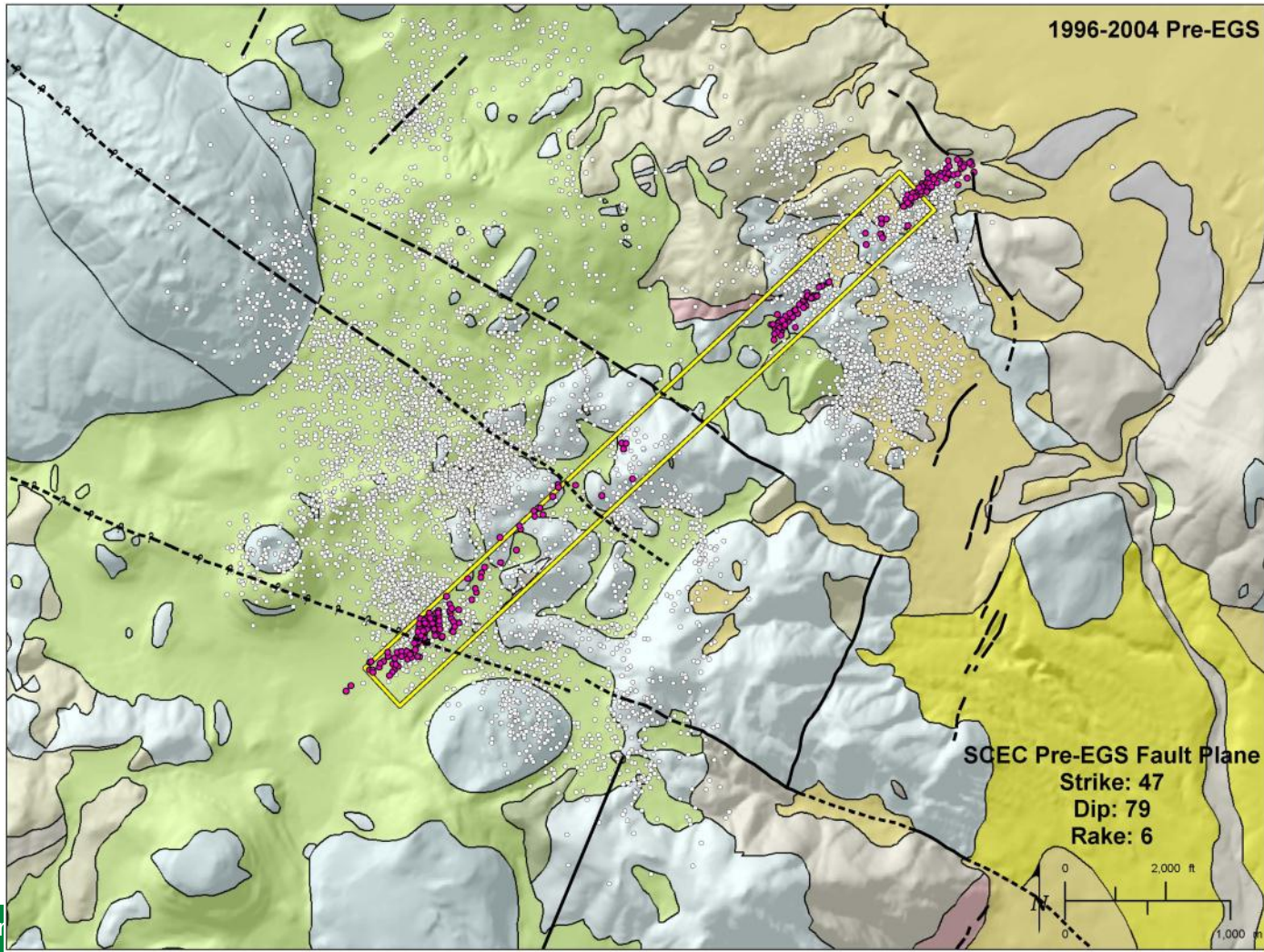
Coso geothermal seismicity is NOT diffuse. 87% occurs within 25 m of planes consistent with tectonic processes along the eastern California shear zone with 83% on vertical and dipping conjugate strike slip planes, 12% normal on planes with dips of 35-70 degrees, and 5% reverse-oblique on steeply-dipping planes. Click on this and next 15 images to animate the different fault planes. (3 of 18) PRE-EGS



Coso geothermal seismicity is NOT diffuse. 87% occurs within 25 m of planes consistent with tectonic processes along the eastern California shear zone with 83% on vertical and dipping conjugate strike slip planes, 12% normal on planes with dips of 35-70 degrees, and 5% reverse-oblique on steeply-dipping planes. Click on this and next 15 images to animate the different fault planes. (4 of 18) PRE-EGS

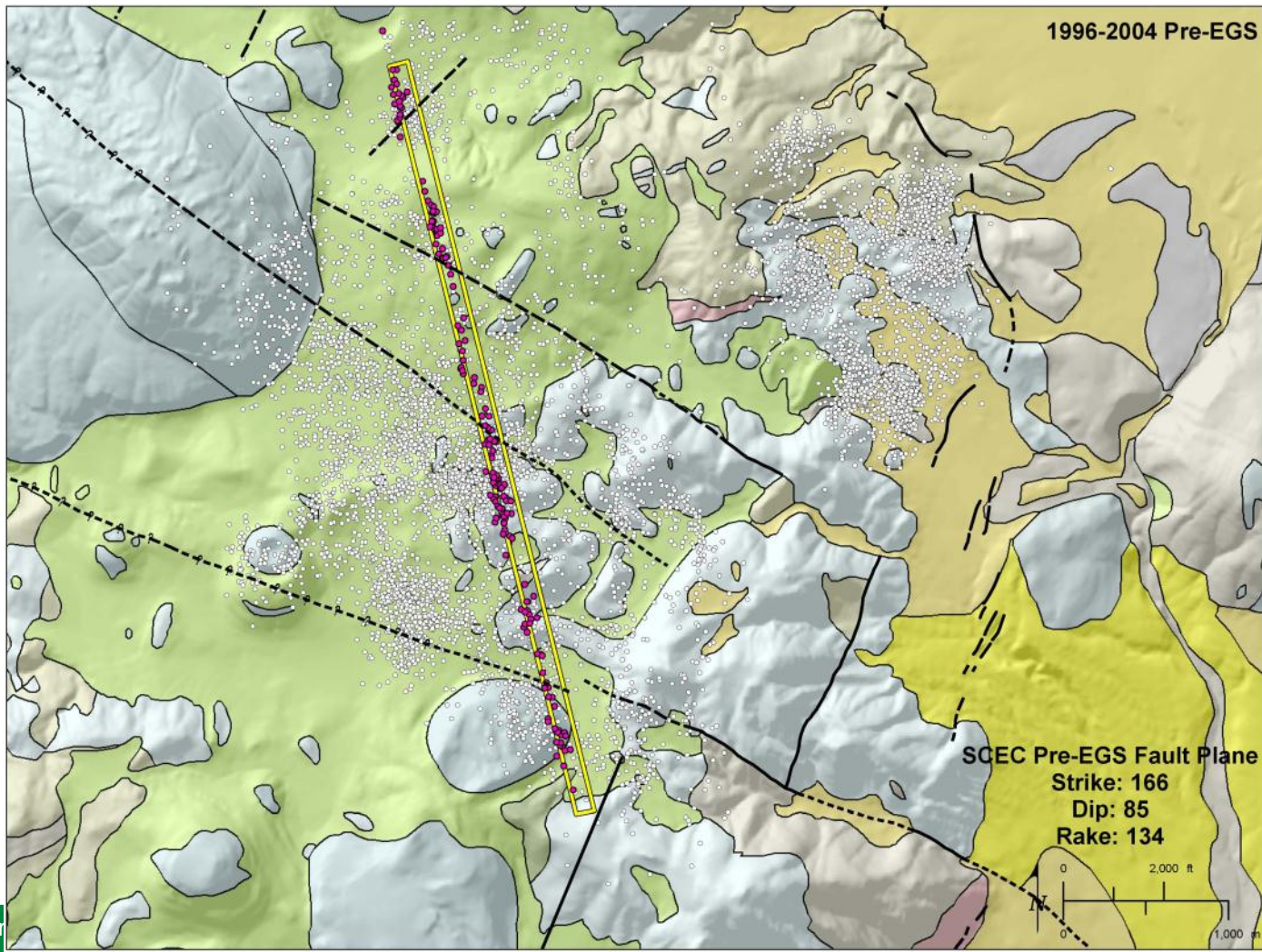


Coso geothermal seismicity is NOT diffuse. 87% occurs within 25 m of planes consistent with tectonic processes along the eastern California shear zone with 83% on vertical and dipping conjugate strike slip planes, 12% normal on planes with dips of 35-70 degrees, and 5% reverse-oblique on steeply-dipping planes. Click on this and next 13 images to animate the different fault planes. (5 of 18) PRE-EGS

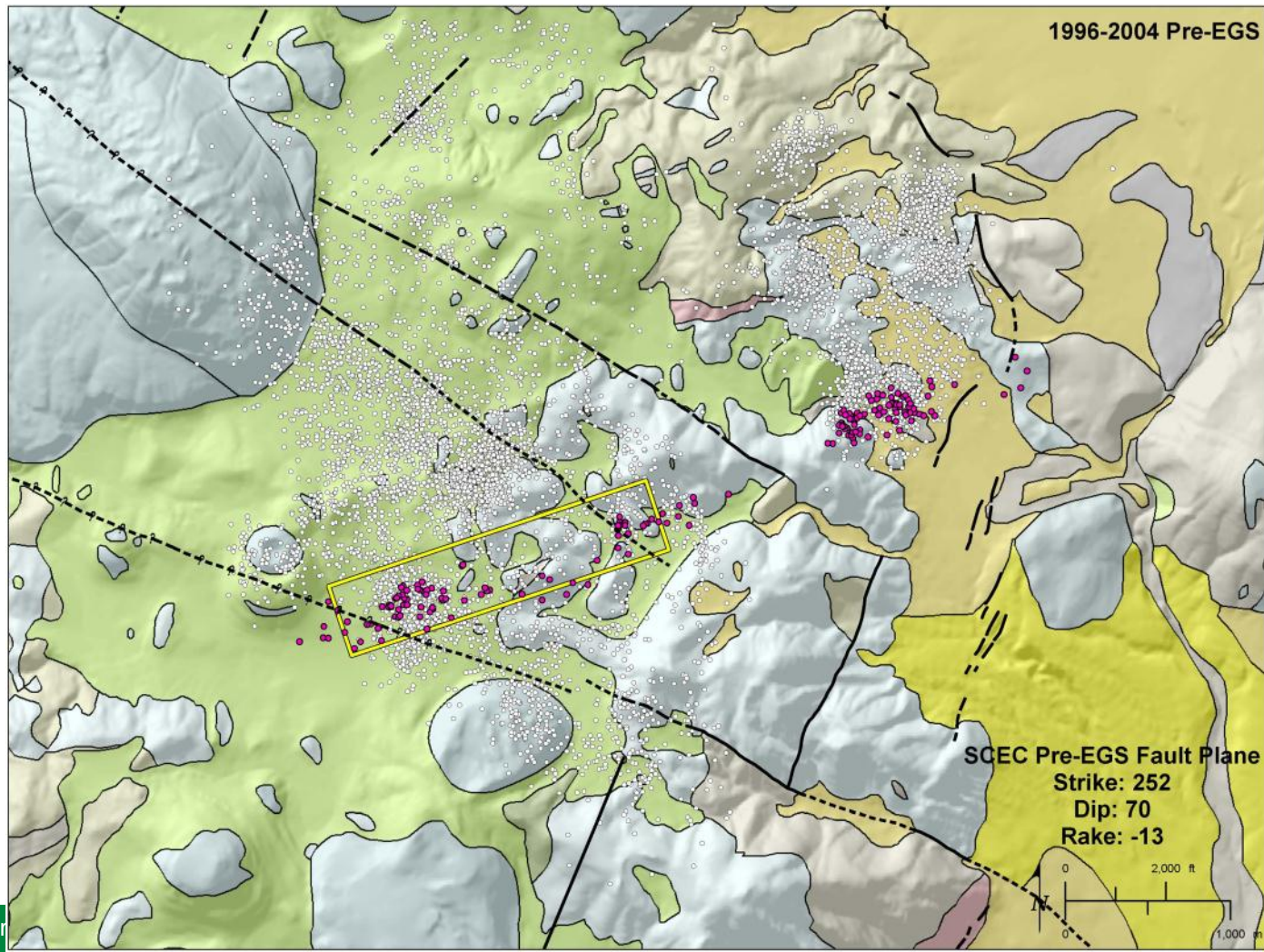


# Accomplishments, Results and Progress

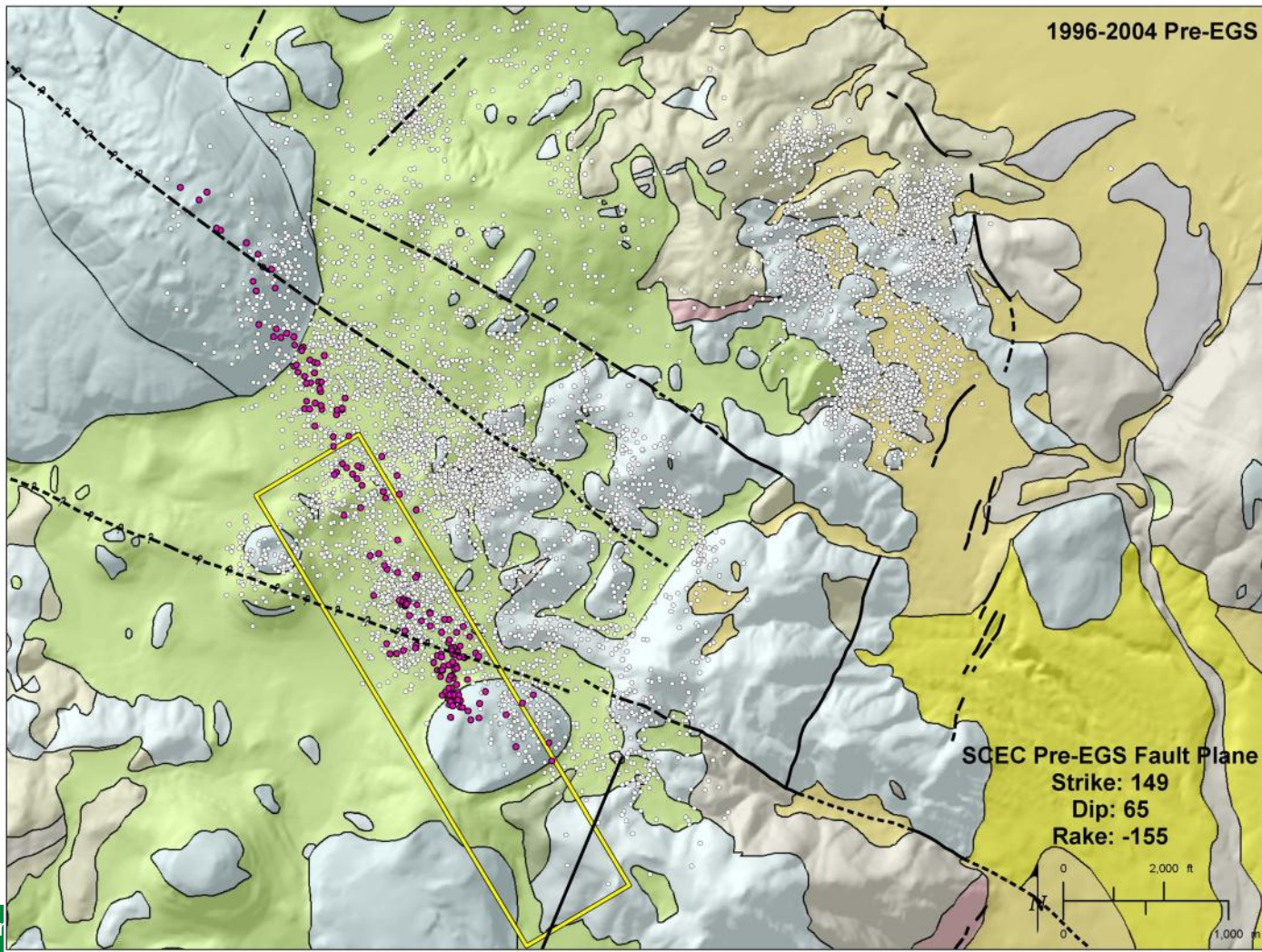
Coso geothermal seismicity is NOT diffuse. 87% occurs within 25 m of planes consistent with tectonic processes along the eastern California shear zone with 83% on vertical and dipping conjugate strike slip planes, 12% normal on planes with dips of 35-70 degrees, and 5% reverse-oblique on steeply-dipping planes. Click on this and next 12 images to animate the different fault planes. (6 of 18) PRE-EGS



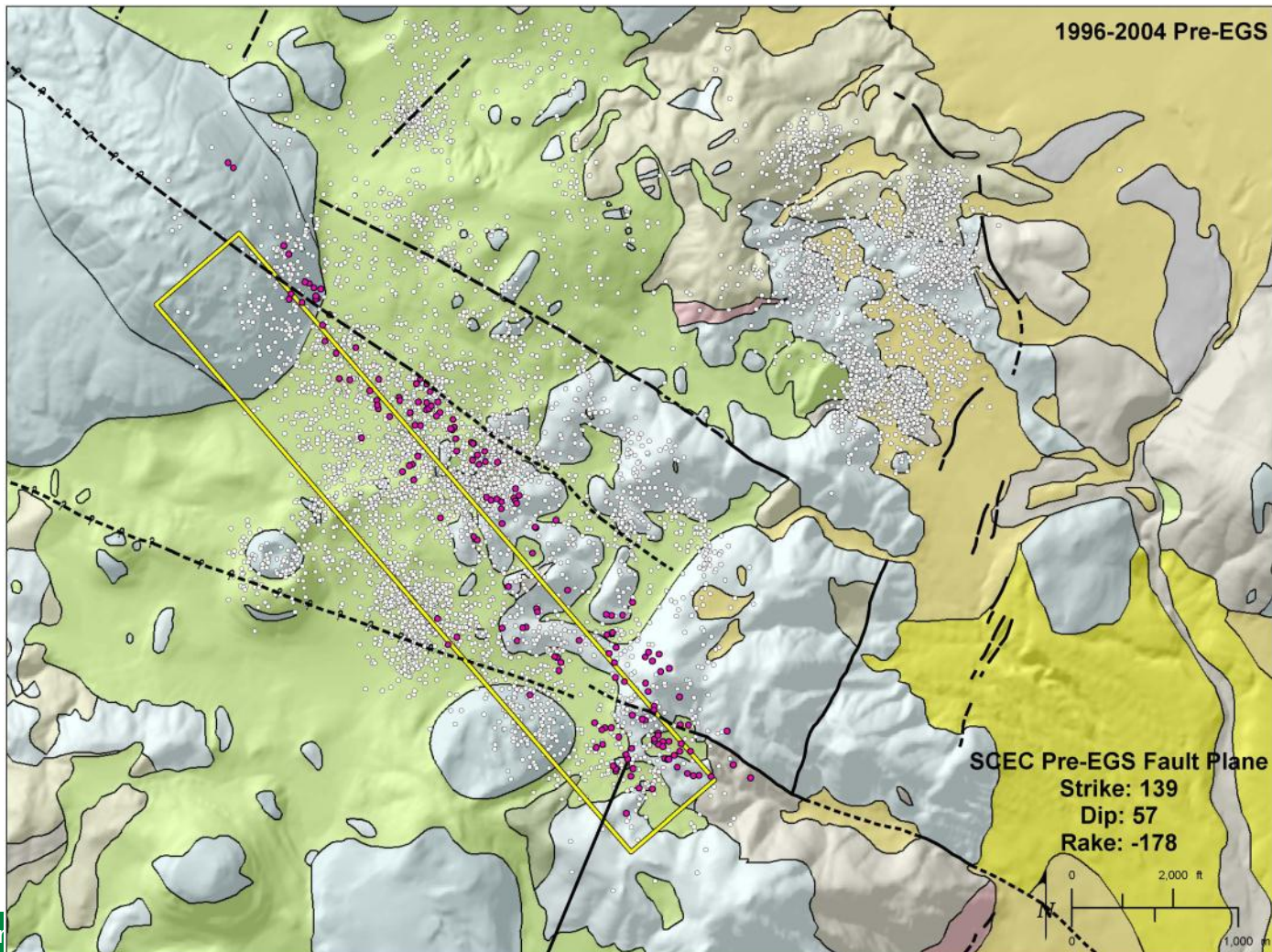
Coso geothermal seismicity is NOT diffuse. 87% occurs within 25 m of planes consistent with tectonic processes along the eastern California shear zone with 83% on vertical and dipping conjugate strike slip planes, 12% normal on planes with dips of 35-70 degrees, and 5% reverse-oblique on steeply-dipping planes. Click on this and next 11 images to animate the different fault planes. (7 of 18) PRE-EGS



Coso geothermal seismicity is NOT diffuse. 87% occurs within 25 m of planes consistent with tectonic processes along the eastern California shear zone with 83% on vertical and dipping conjugate strike slip planes, 12% normal on planes with dips of 35-70 degrees, and 5% reverse-oblique on steeply-dipping planes. Click on this and next 10 images to animate the different fault planes. (8 of 18) PRE-EGS

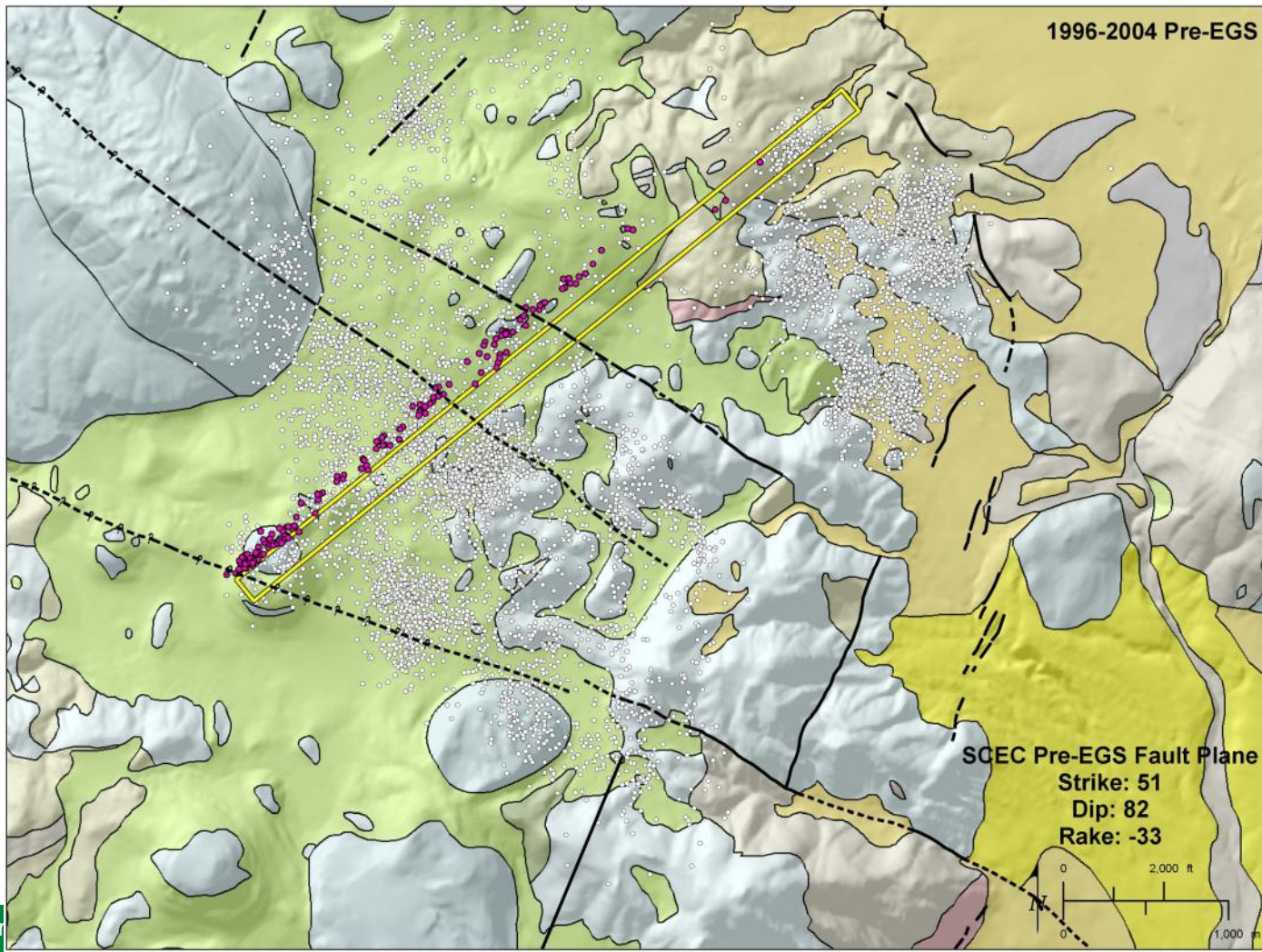


Coso geothermal seismicity is NOT diffuse. 87% occurs within 25 m of planes consistent with tectonic processes along the eastern California shear zone with 83% on vertical and dipping conjugate strike slip planes, 12% normal on planes with dips of 35-70 degrees, and 5% reverse-oblique on steeply-dipping planes. Click on this and next 9 images to animate the different fault planes. (9 of 18) PRE-EGS

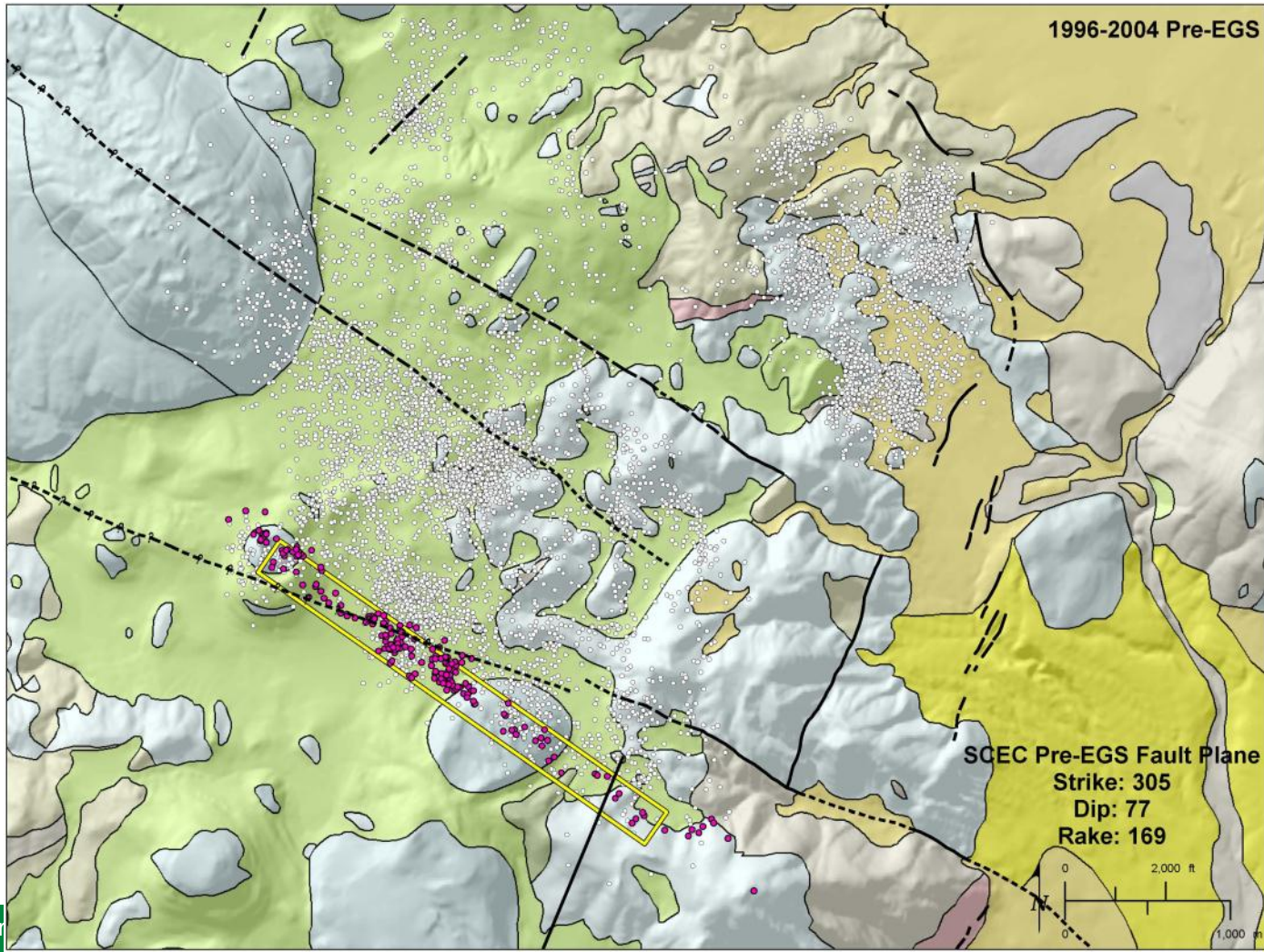


# Accomplishments, Results and Progress

Coso geothermal seismicity is NOT diffuse. 87% occurs within 25 m of planes consistent with tectonic processes along the eastern California shear zone with 83% on vertical and dipping conjugate strike slip planes, 12% normal on planes with dips of 35-70 degrees, and 5% reverse-oblique on steeply-dipping planes. Click on this and next 8 images to animate the different fault planes. (10 of 18) PRE-EGS

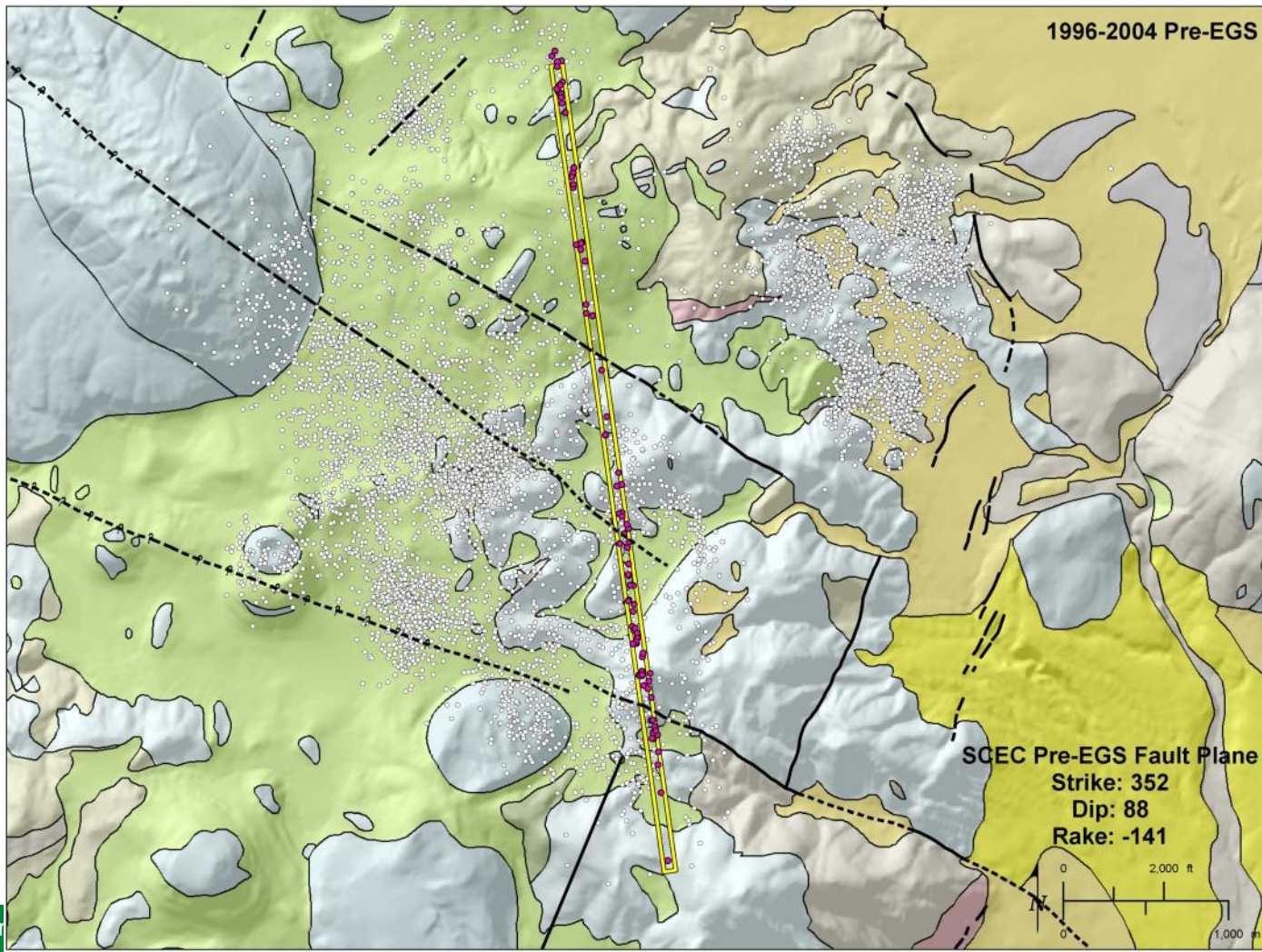


Coso geothermal seismicity is NOT diffuse. 87% occurs within 25 m of planes consistent with tectonic processes along the eastern California shear zone with 83% on vertical and dipping conjugate strike slip planes, 12% normal on planes with dips of 35-70 degrees, and 5% reverse-oblique on steeply-dipping planes. Click on this and next 7 images to animate the different fault planes. (11 of 18) PRE-EGS

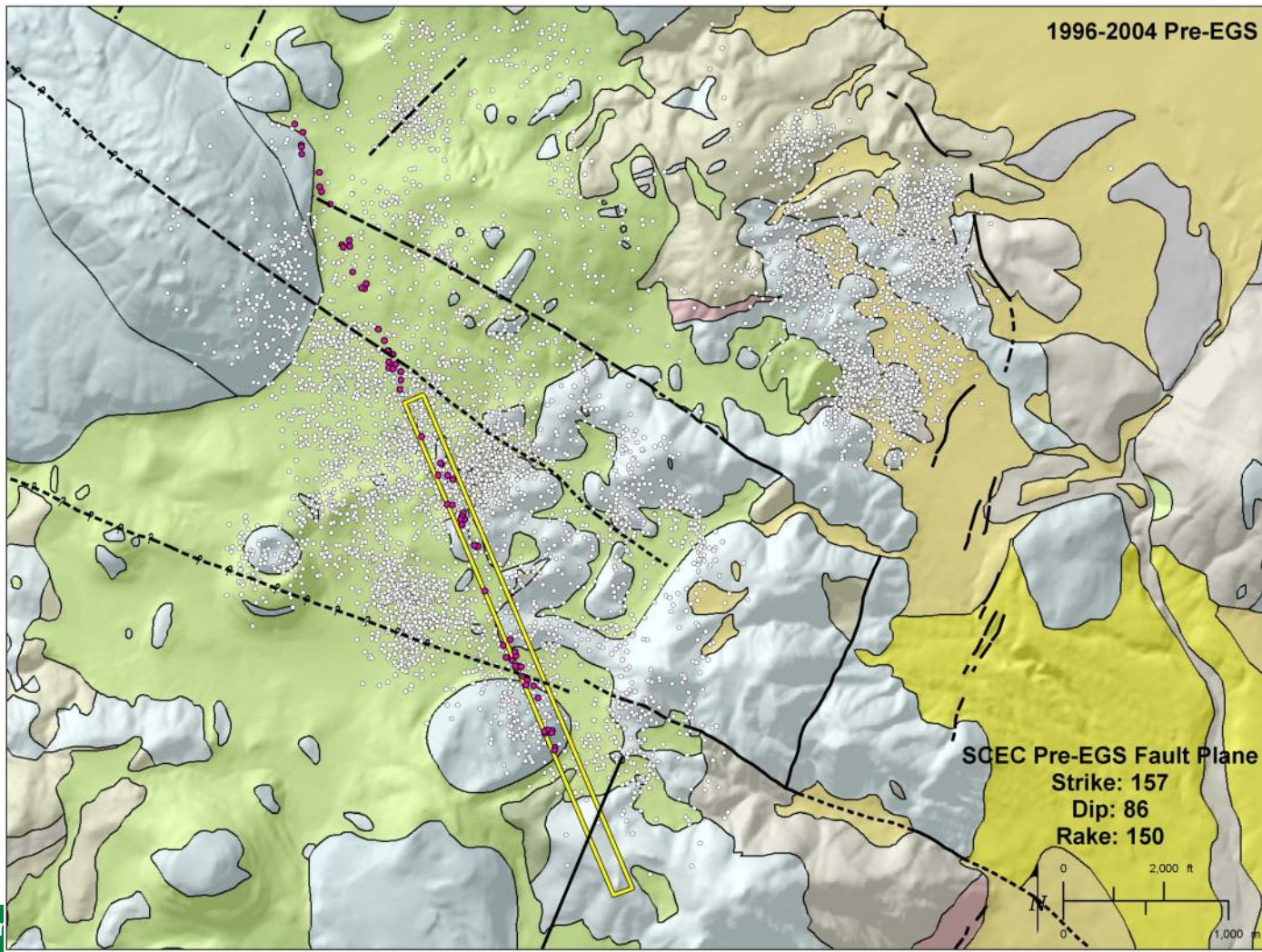


# Accomplishments, Results and Progress

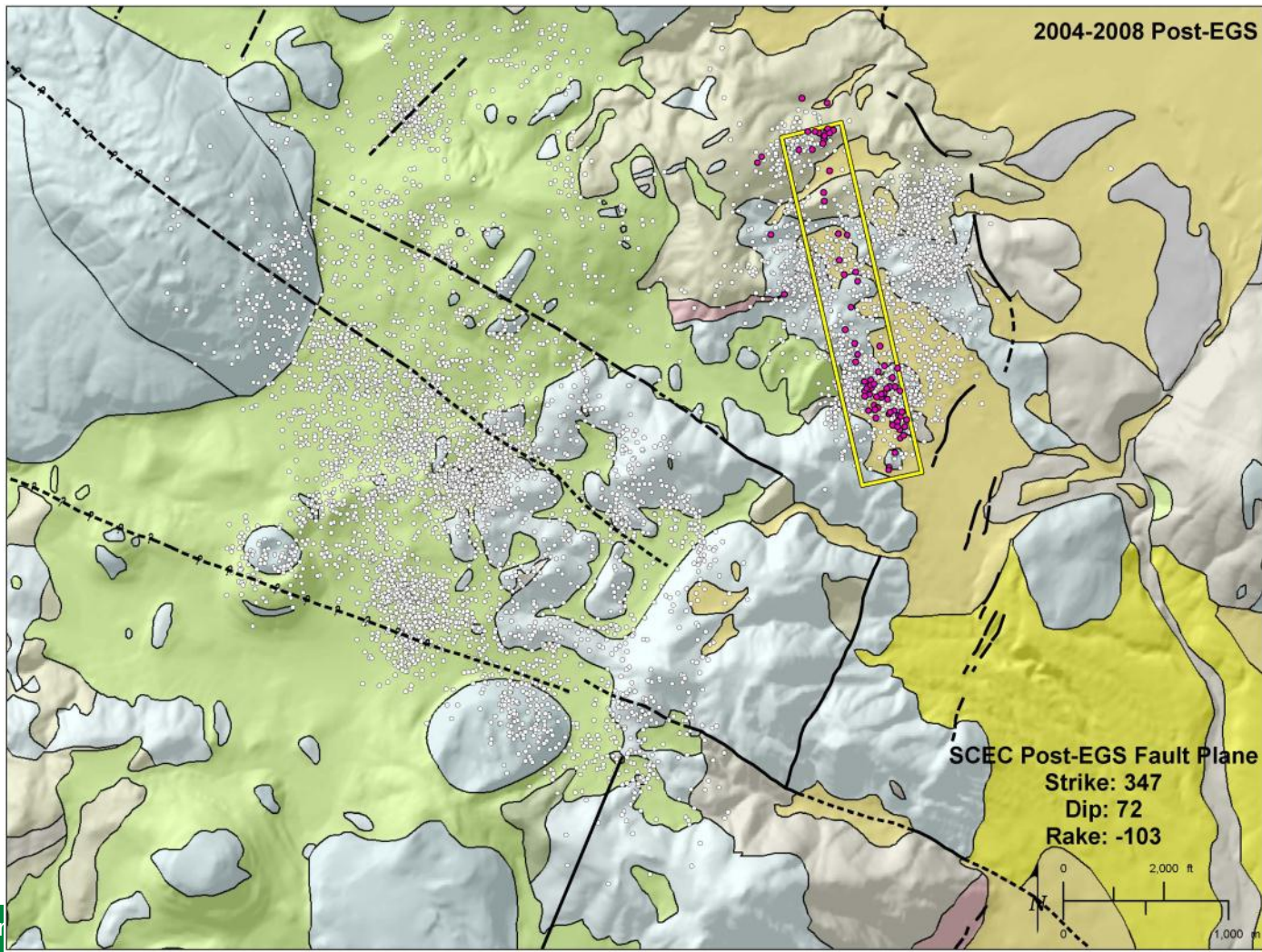
Coso geothermal seismicity is NOT diffuse. 87% occurs within 25 m of planes consistent with tectonic processes along the eastern California shear zone with 83% on vertical and dipping conjugate strike slip planes, 12% normal on planes with dips of 35-70 degrees, and 5% reverse-oblique on steeply-dipping planes. Click on this and next 6 images to animate the different fault planes. (12 of 18) PRE-EGS



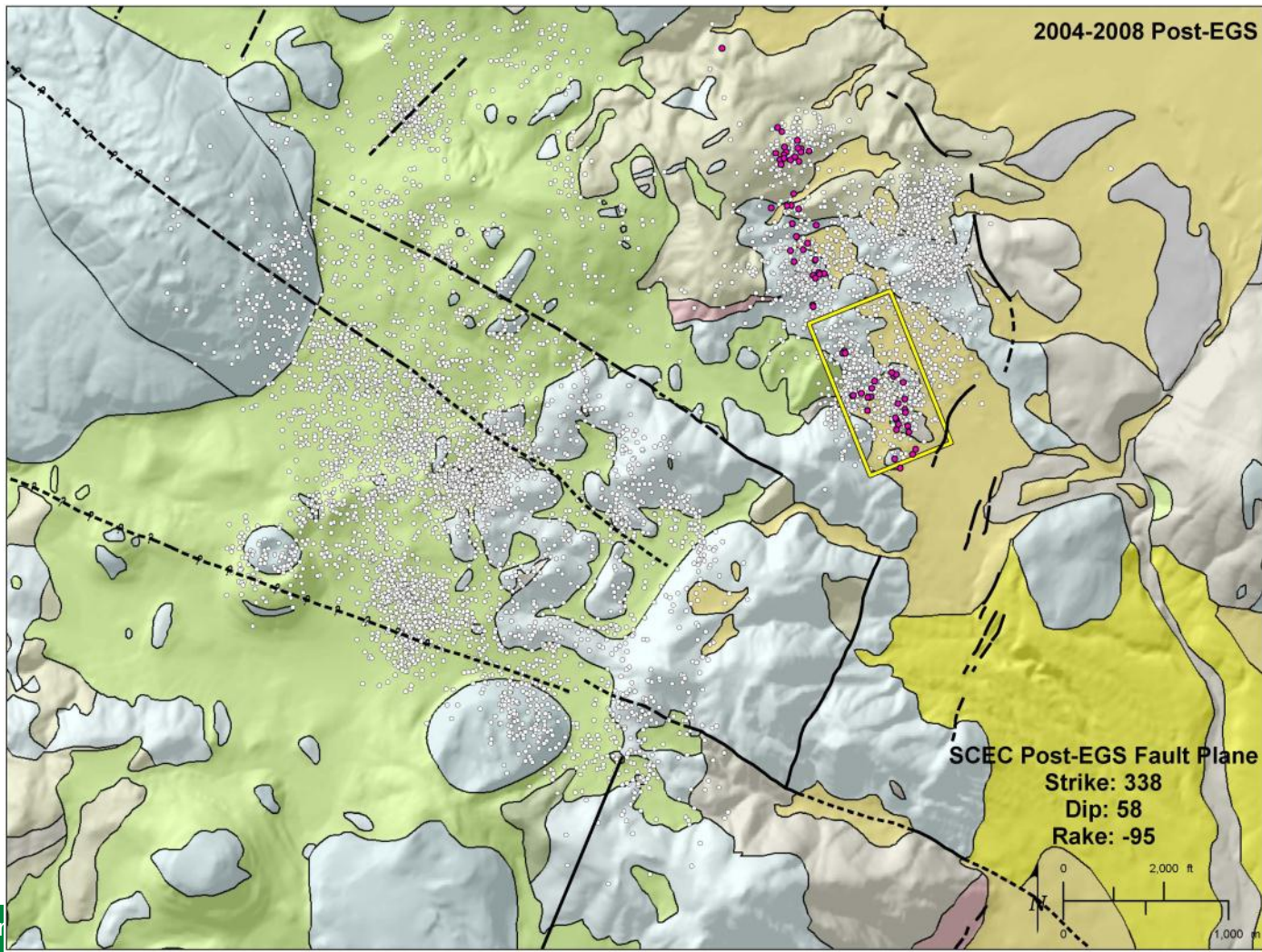
Coso geothermal seismicity is NOT diffuse. 87% occurs within 25 m of planes consistent with tectonic processes along the eastern California shear zone with 83% on vertical and dipping conjugate strike slip planes, 12% normal on planes with dips of 35-70 degrees, and 5% reverse-oblique on steeply-dipping planes. Click on this and next 5 images to animate the different fault planes. (13 of 18). PRE-EGS



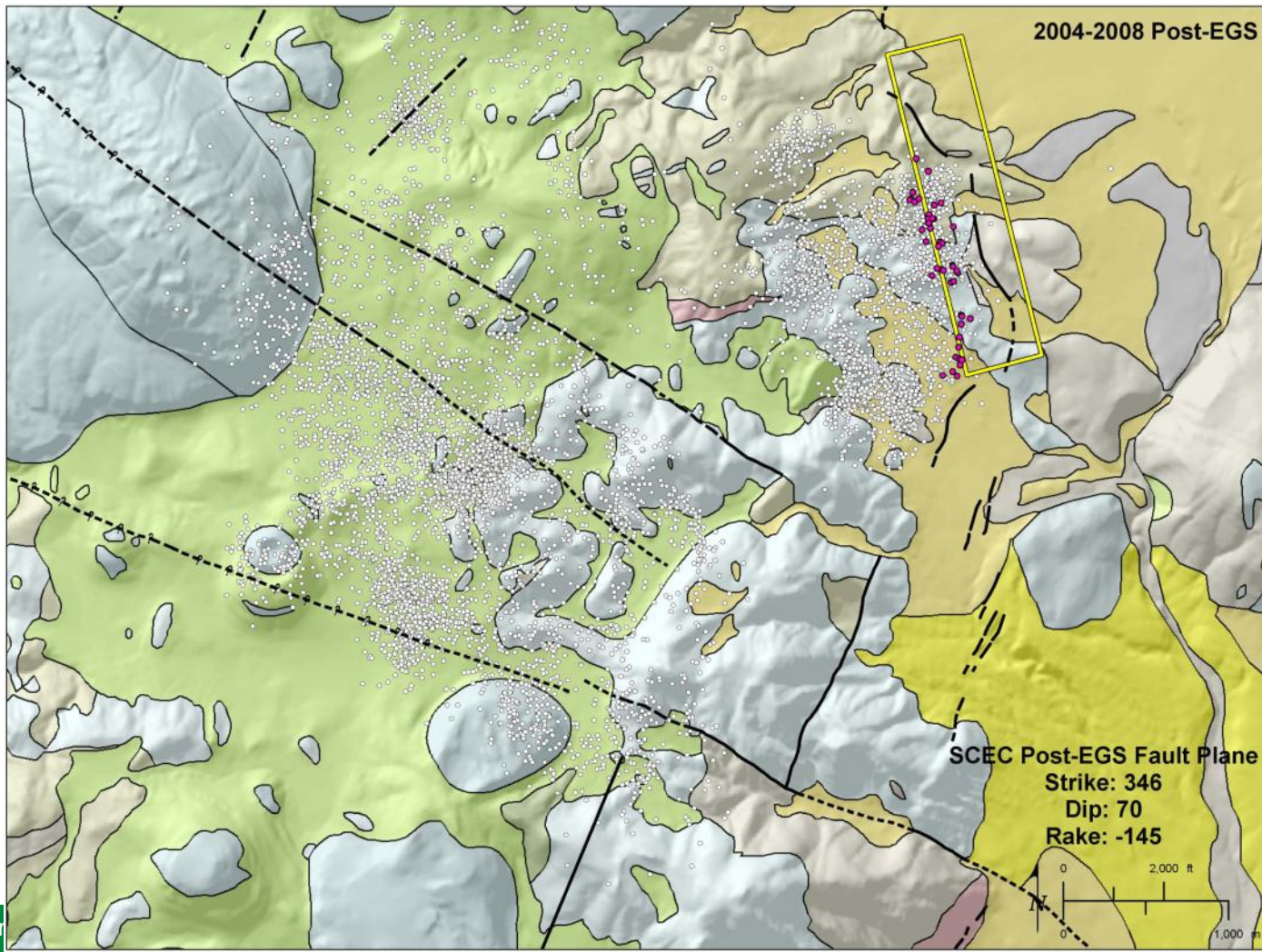
Coso geothermal seismicity is NOT diffuse. 87% occurs within 25 m of planes consistent with tectonic processes along the eastern California shear zone with 83% on vertical and dipping conjugate strike slip planes, 12% normal on planes with dips of 35-70 degrees, and 5% reverse-oblique on steeply-dipping planes. Click on this and next 4 images to animate the different fault planes. (14 of 18). POST-EGS



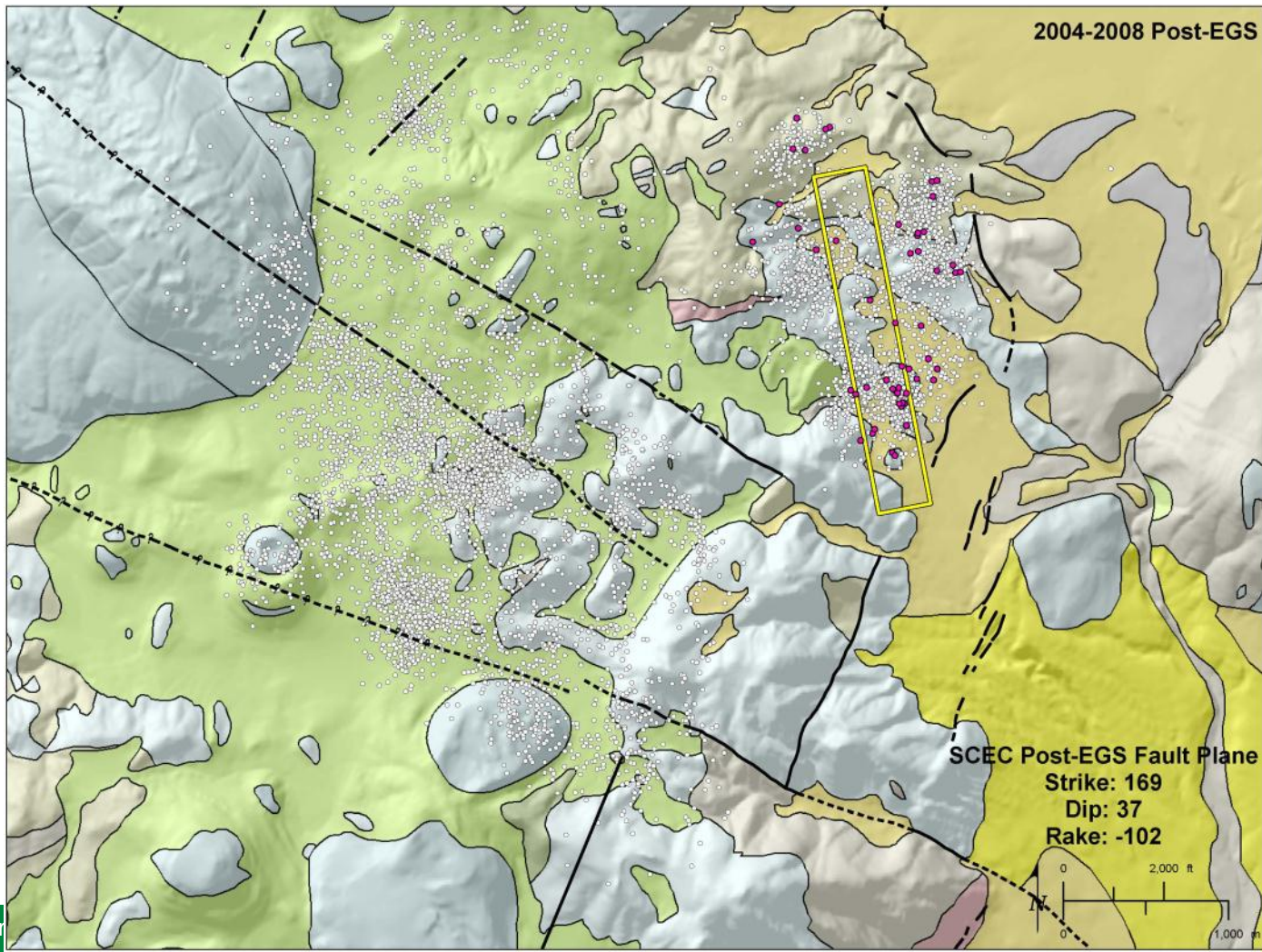
Coso geothermal seismicity is NOT diffuse. 87% occurs within 25 m of planes consistent with tectonic processes along the eastern California shear zone with 83% on vertical and dipping conjugate strike slip planes, 12% normal on planes with dips of 35-70 degrees, and 5% reverse-oblique on steeply-dipping planes. Click on this and next 3 images to animate the different fault planes. (15 of 18). POST-EGS



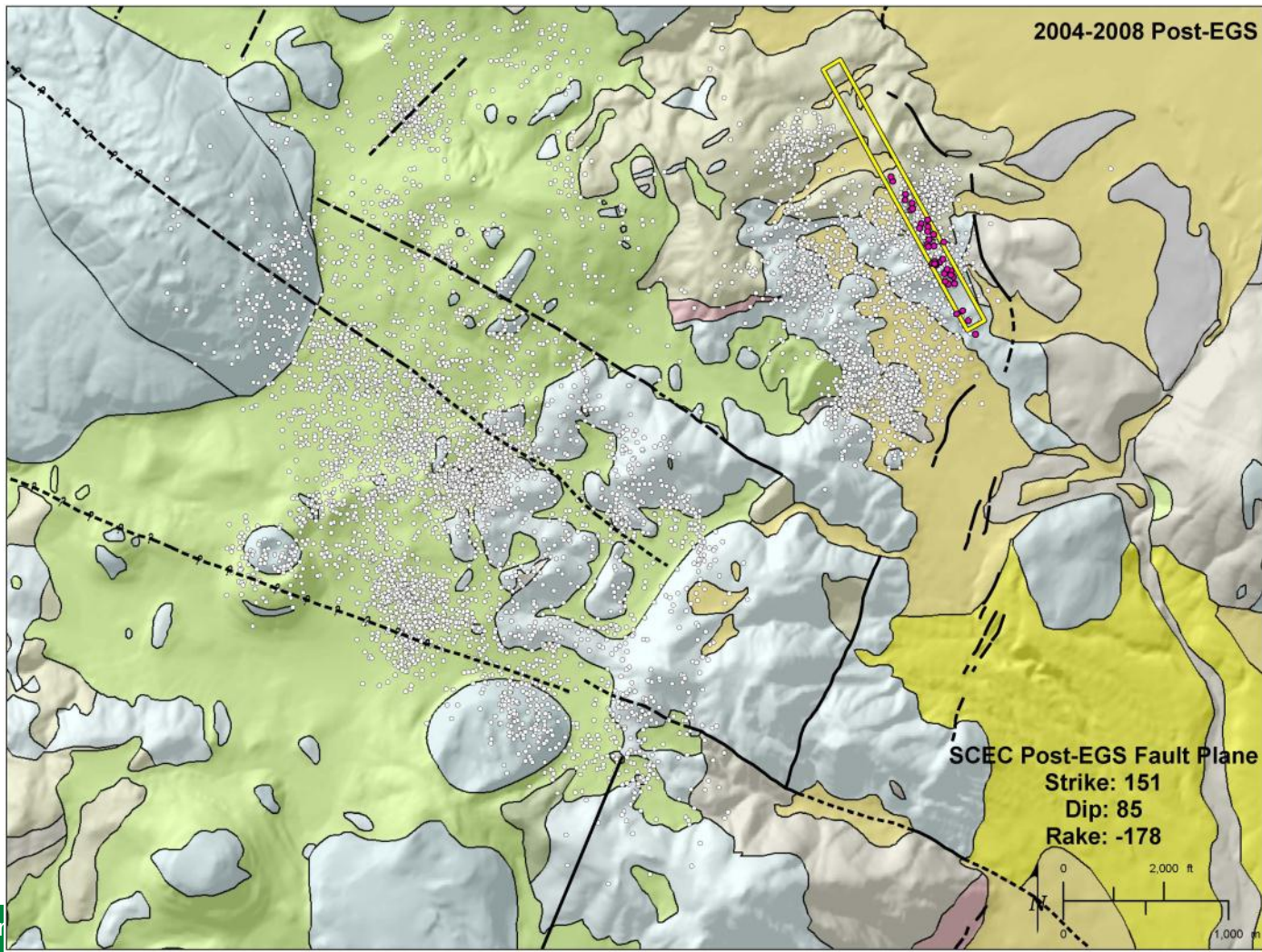
Coso geothermal seismicity is NOT diffuse. 87% occurs within 25 m of planes consistent with tectonic processes along the eastern California shear zone with 83% on vertical and dipping conjugate strike slip planes, 12% normal on planes with dips of 35-70 degrees, and 5% reverse-oblique on steeply-dipping planes. Click on this and next 2 images to animate the different fault planes. (16 of 18). POST-EGS



Coso geothermal seismicity is NOT diffuse. 87% occurs within 25 m of planes consistent with tectonic processes along the eastern California shear zone with 83% on vertical and dipping conjugate strike slip planes, 12% normal on planes with dips of 35-70 degrees, and 5% reverse-oblique on steeply-dipping planes. Click on this and next image to animate the different fault planes. (17 of 18). POST-EGS

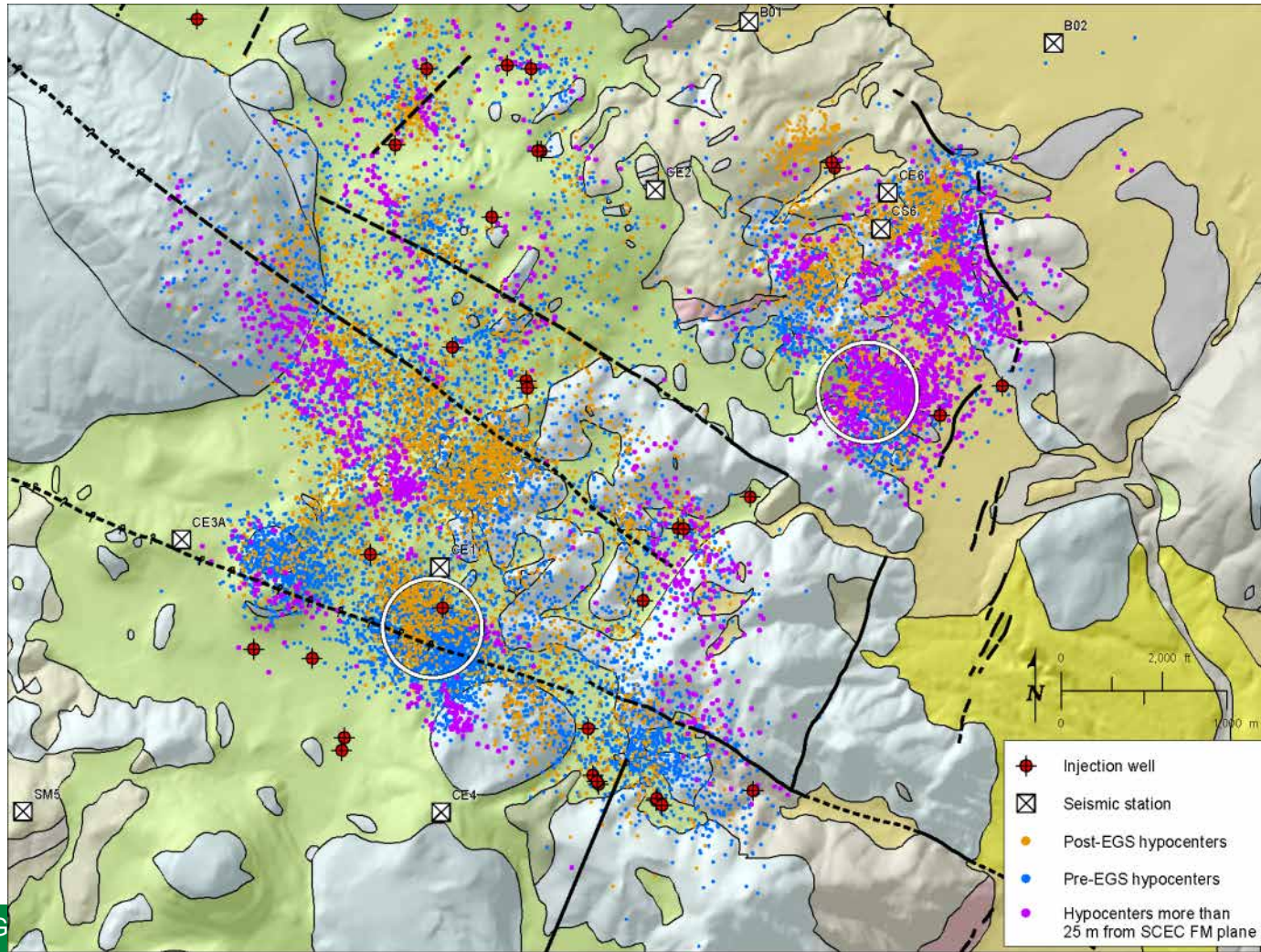


Coso geothermal seismicity is NOT diffuse. 87% occurs within 25 m of planes consistent with tectonic processes along the eastern California shear zone with 83% on vertical and dipping conjugate strike slip planes, 12% normal on planes with dips of 35-70 degrees, and 5% reverse-oblique on steeply-dipping planes. Last image in the animation of the different fault planes. (18 of 18). POST-EGS

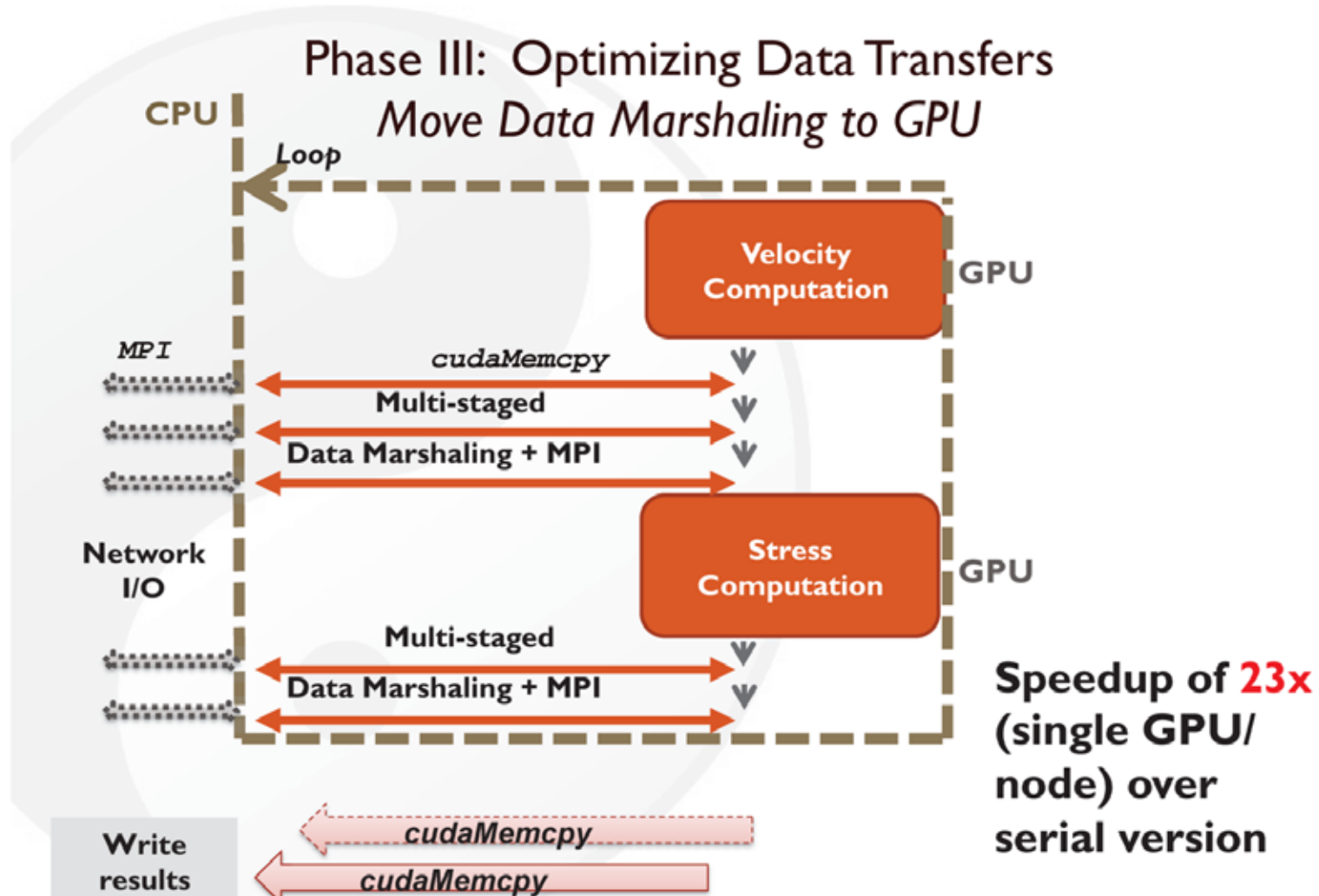


# Accomplishments, Results and Progress

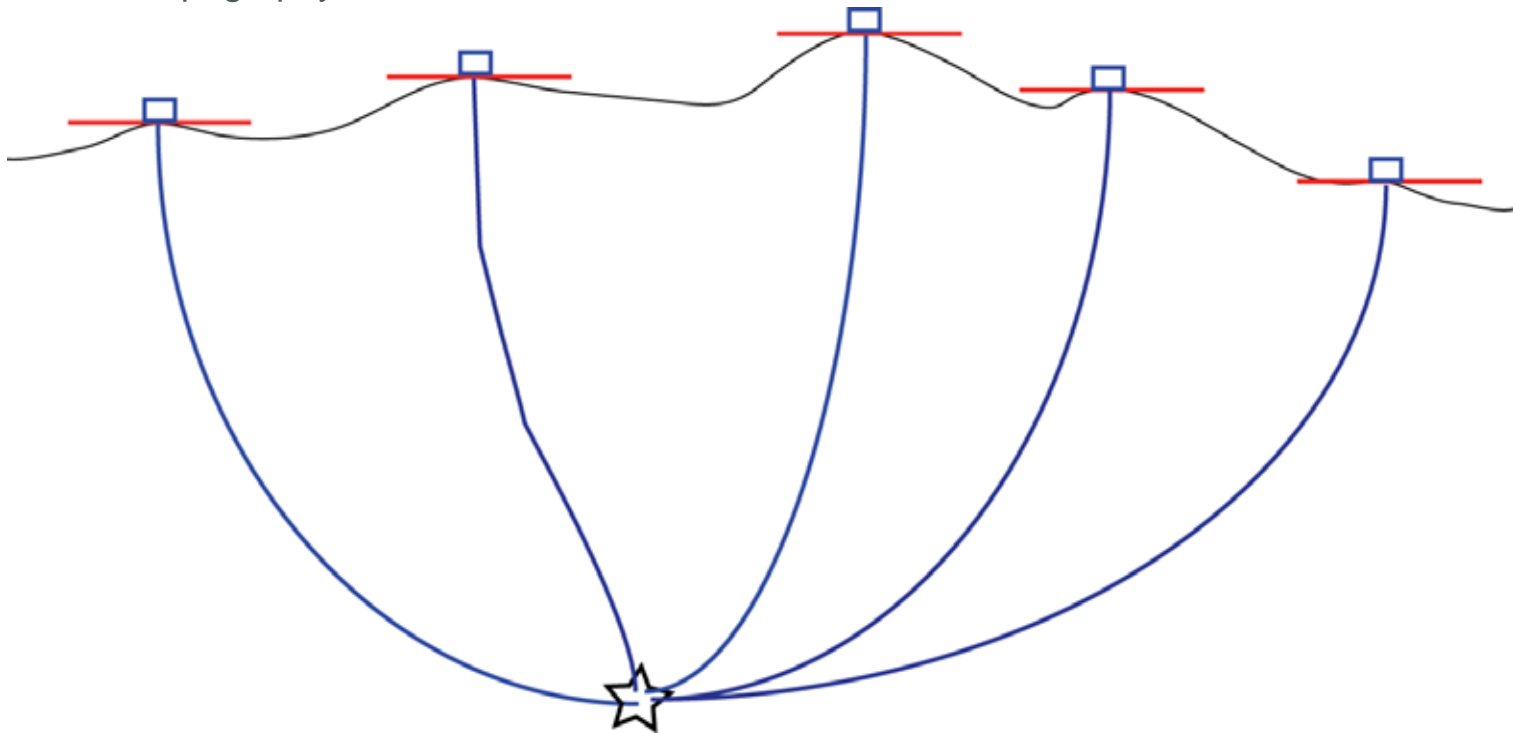
Coda-wave interferometry identifies two region of the Coso geothermal field where velocities decreased 0.1%-0.2% near injection wells, including the 2004-2005 EGS injection test site. Velocities increased 0.1%-0.2% several years later resulting in no net remaining velocity change. We are working with Terra-Gen to integrate injection histories and other well data into the analyses of these velocity changes.



Initial scalar GPU optimization of “disfd”



Reciprocity “disfd”, development and validation of fast 3D fourth-order variable-mesh viscoelastic finite difference waveform kernel calculation with topography. 87% reduction in memory required relative to fixed mesh, reduced run time because time step can be increased by a factor of three and spatial computations are reduced by a factor of 8. Speedup per GPU is 40-50 times relative to CPU. Reciprocity allows calculation of kernels for all earthquakes in a single 3D calculation for each station component. This reciprocity combined with data functionals that allow precise specification of time and frequency windows for inversion allow fast calculation of waveform inversion kernels for P- and S-wave direct wave windows with topography.



Development and validation of fast 3D fourth-order variable-mesh viscoelastic finite difference waveform kernel calculation with topography.

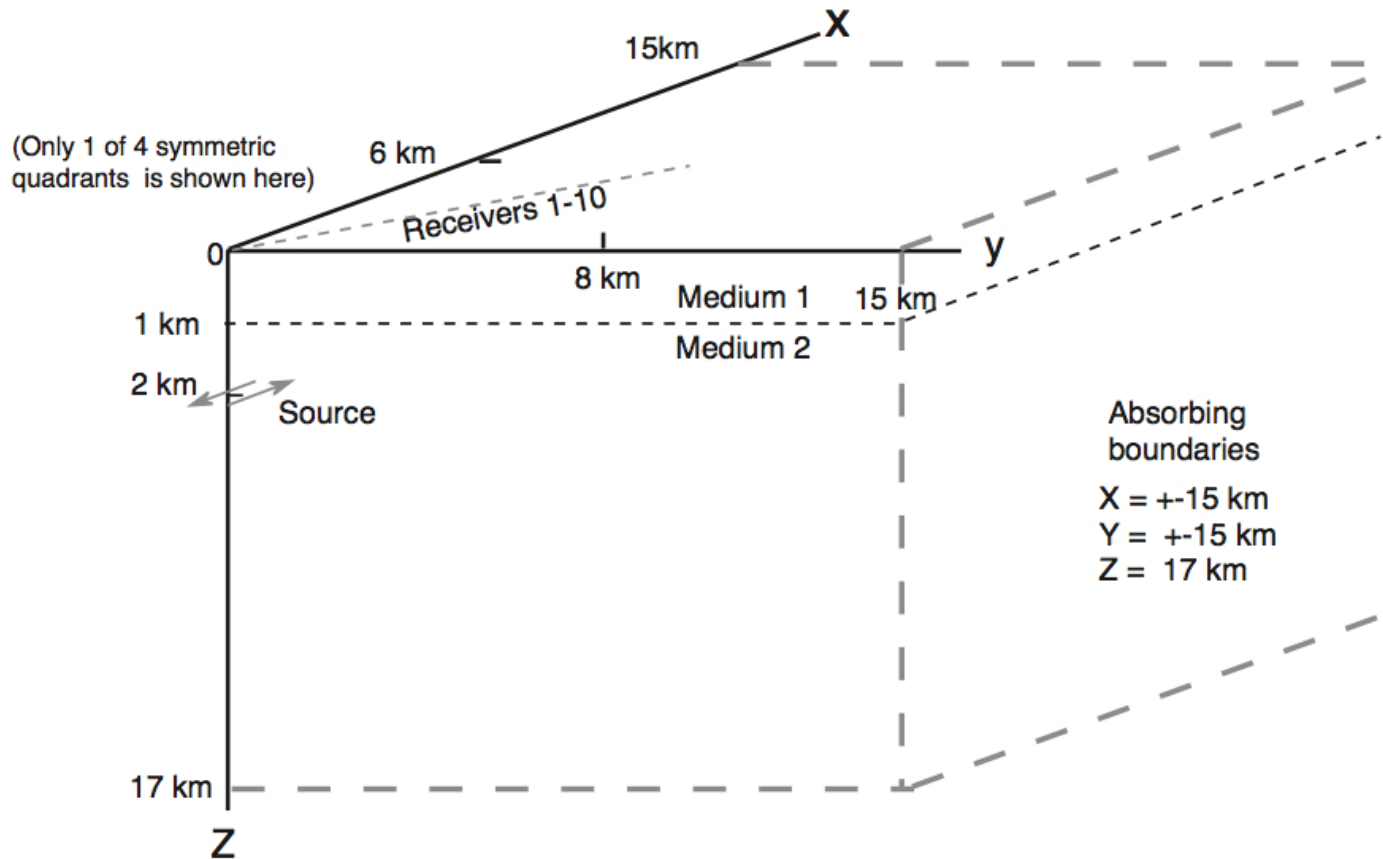
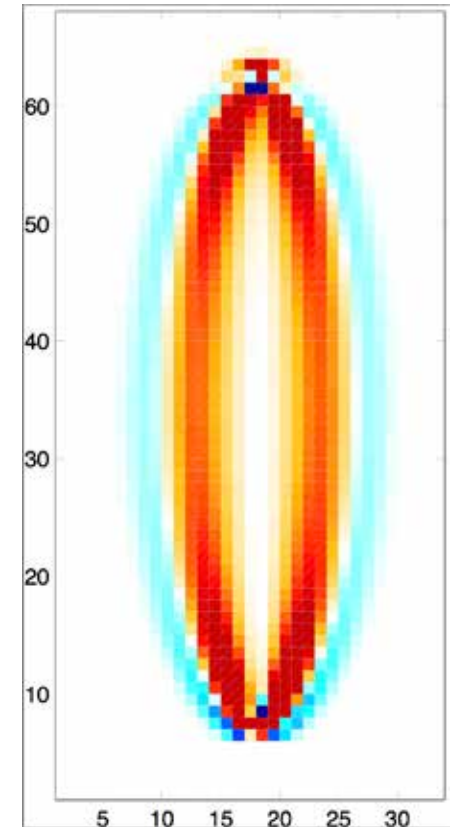
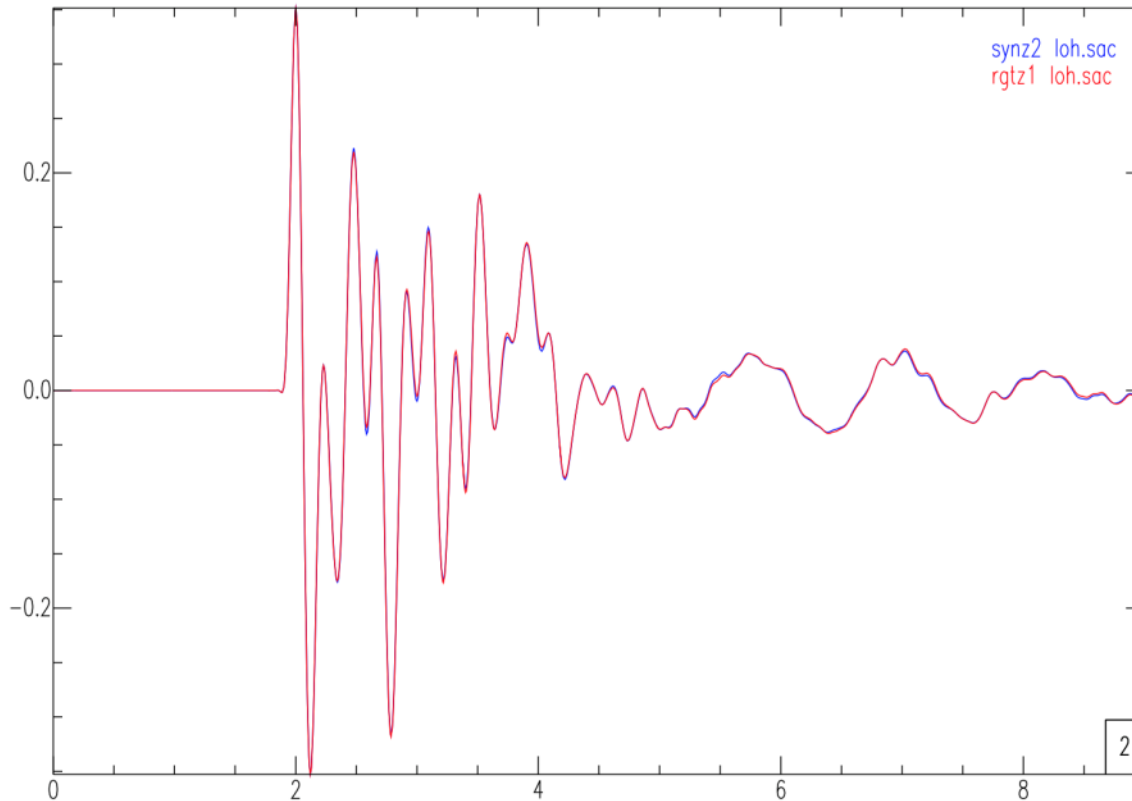


**Figure 1.** Problem setup for the test case LOH.1 as shown in Day (2001).

Development and validation of fast 3D fourth-order variable-mesh viscoelastic finite difference waveform kernel calculation with topography. (Left) Vertical component synthetic seismogram computed through the forward simulation that propagates the wave from the source to the receiver (blue) and through the reciprocal calculation that combines the moment tensor with the receiver-side strain Green's tensor at the source location (red). Map-view plot of the sensitivity kernel at the source-receiver depth (right).



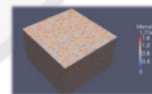
- Invert coda wave data for the real magnitude of a localized velocity change from estimated travel time shifts using multiple-scattered wave sensitivity kernels. Supported past project end by CSM Center for Wave Propagation funding
  - Validate and apply Dr. Block's generalized inversion approach to convert relative-times to precise absolute times with Paradox and Coso data.
  - Complete the MPI/GPU waveform inversion validations and apply to Paradox and Newberry EGS earthquake data to estimate moment tensors and 3D velocity structure. Demonstrate near real-time waveform assimilation capabilities with the Newberry EGS earthquake data. Will use additional matching funds from Fugro for Newberry demonstration.
  - Complete modifications to open-source fast-marching 3D inversion code to include surface-wave dispersion constraints in 3D velocity-hypocenter inversion.
  - Apply coupled poro-elastic analyses to 2012 Newberry EGS testing data.
- Once we determined that 3D waveform inversion was feasible we focused on providing fast, robust tools, for all phases (phase picking, travel-time inversion, stress estimation) to provide the near-real-time analysis capabilities required to support an ongoing EGS injection testing program

Virginia Tech provides key computer science resources to ensure maximum parallel speed is achieved (all aspects of the problem are parallelized including I/O).

Exploit the gaming GPU to simultaneously output visualization during computations to monitor progress and accuracy in near real time.

## Phase IV: Towards In-Situ Visualization

- ☒ In-Situ Visualization
  - ☒ Visualize the simulation *as it progresses* in (near) real time.
- ☒ Benefit
  - ☒ Assists in the early detection of errors as the simulation progresses ... rather than wait for the entire simulation to run and be rendered as a movie before errors can be identified.
- ☒ Approach
  - ☒ Directly read the physical properties of the simulation (e.g., velocity vectors, stress tensors etc.) from GPU buffers.
  - ☒ Immediately render and transmit to the GPU screen frame buffers for (near) real-time visualization, e.g., HokieWall



- Coda-wave interferometry detects velocity changes associated with injection. Research will continue beyond project end date with separate funding.
- Regularized ambient-noise and stationary-phase earthquake deconvolution provide surface wave dispersion to 5 Hz to constrain shallow velocity structure.
- Bayesian S-wave picking and generalized inversion of cross-correlation relative times for high-accuracy absolute times improves absolute hypocenter resolution to locate wells in relation to earthquakes and fractures.
- Developed and commercialized fast 3D waveform inversion capabilities available from multiple companies that account for topography that runs on inexpensive gaming GPU PCs making overnight waveform inversion during EGS injection activities an inexpensive option.
- Reduced the costs of seismic monitoring with increased resolution.
- Produced 3D finite element fully-coupled poro-elastic modeling that provides a fast accurate tool to assess seismogenic potential.

Timeline:

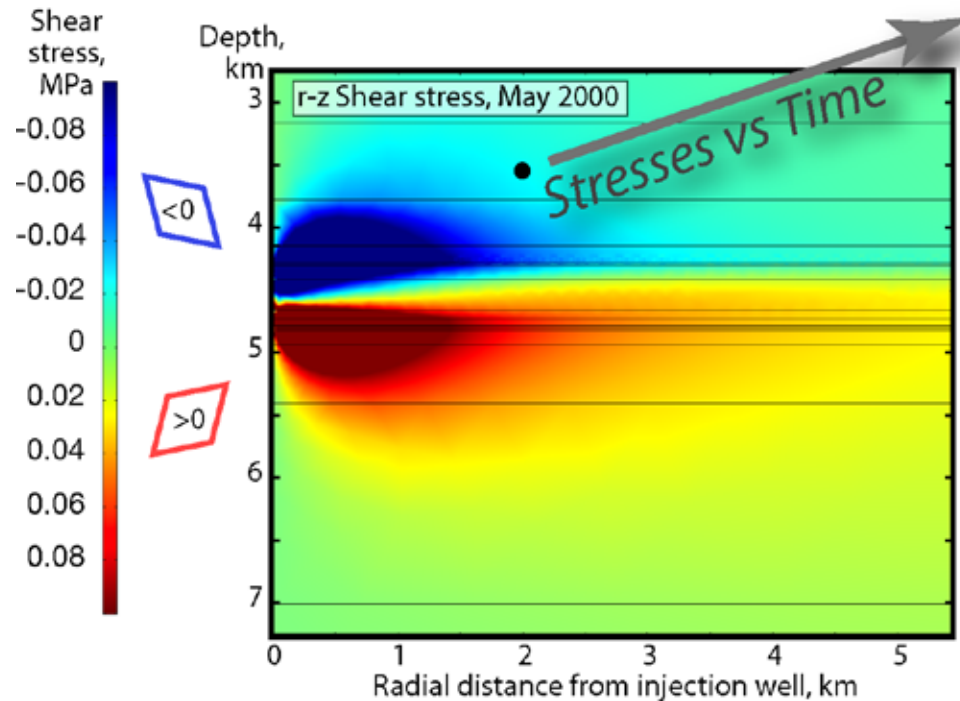
| Planned Start Date | Planned End Date | Actual Start Date                     | Current End Date |
|--------------------|------------------|---------------------------------------|------------------|
| 1/29/2010          | 12/31/2012       | 3/27/2010 (full funding<br>8/20/2010) | 9/30/2013        |

Budget:

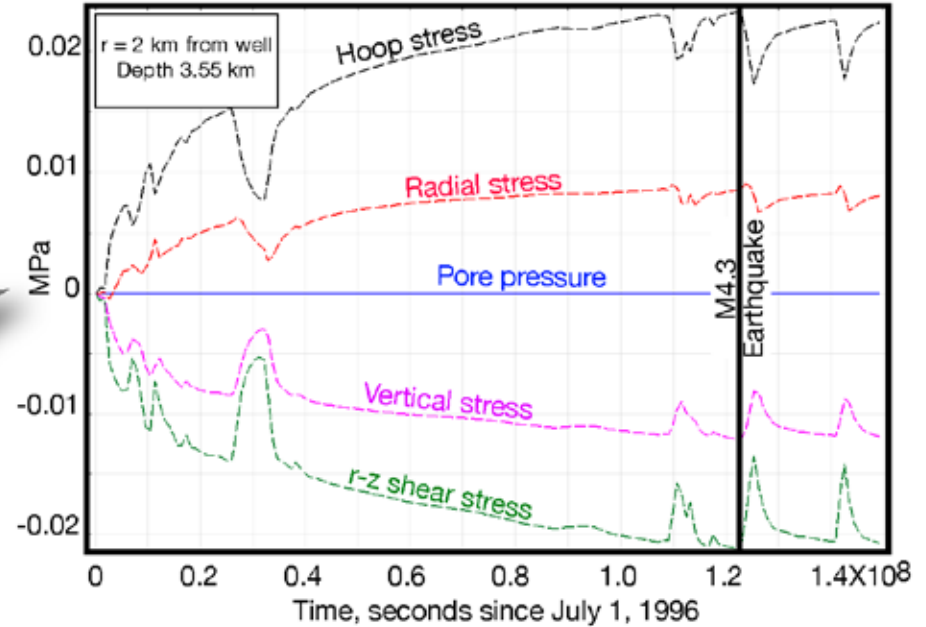
| Federal Share | Cost Share | Planned Expenses to Date | Actual Expenses to Date | Value of Work Completed to Date | Funding needed to Complete Work |
|---------------|------------|--------------------------|-------------------------|---------------------------------|---------------------------------|
| \$1,093,235   | \$313,510  | \$700,000                | \$617,591               | \$617,591                       | \$515,000                       |

- Fugro is providing funds to assist in the commercialization of Fullwave Technologies to provide long-term commercial availability of full waveform inversion capabilities for the geothermal industry.
- This project has benefited from my participation in large-scale crustal seismic fault imaging using oil/gas 3D technology with active and passive sources.
- Previous peer-reviewed recommended more consistent and broader collaboration and application within the geothermal industry. After the last peer review we hired a senior geologist/project manager that has engaged multiple geothermal contacts in research and industry to move our technology more quickly into important geothermal applications.
- Please provide recommendations for increasing the value of our work in geothermal applications.

## Shear stress due to injection



## Stress tensor above injection zone



*Paradox axisymmetric COMSOL model*